results suggested that cPKC plays a crucial role in K^+-induced DA release machinery in PC12 cells.

βPIX KD suppressed DA release

Because βPIX is able to stimulate growth hormone secretion from PC12 cells (Momboisse et al., 2009; Momboisse et al., 2010), we investigated the possible relationship between βPIX and DA release. KD of βPIX in PC12 cells by shRNA (sh369) resulted in a significant inhibition of K^+-evoked DA secretion from PC12 cells (Fig. 7*B*). A similar significant reduction in DA release was reproduced with synthetic βPIX siRNA (Fig. 7*C*). These results were consistent with the idea that βPIX is an important element of the DA exocytotic machinery.

PKC-mediated phosphorylation of β2PIX at Ser340 and Ser583 promoted DA release

To determine the role of the PKC-mediated phosphorylation of βPIX in DA release, we exogenously and simultaneously introduced the shRNA-resistant forms of β2PIX mutant, including β2PIX Thr76Ala, Ser340Ala, or Ser583Ala mutants and βPIX sh369, into PC12 cells. DA release from PC12 cells transfected with sh369 was completely rescued by the reintroduction of WT FLAG-tagged β2PIX (Fig. 8*A*). These results suggested that β2PIX, which is a dominant isoform in the CNS, has important roles in DA release. Moreover, we examined the effects of the β2PIX phosphorylation on DA release. β2PIX Ser340Ala and Ser583Ala mutants failed to rescue the reduced DA release by βPIX sh369, whereas the β2PIX Thr76Ala mutant acted similarly to WT β2PIX (Fig. 8*A*). Together, our results suggested that the PKC-mediated phosphorylation of Ser340 and Ser583 on β2PIX positively regulates DA release. Finally, we examined the effects of Cdc42 and Rac1 KD on DA release. When Cdc42 was knocked down, Rac1 was upregulated and vice versa. Therefore, we knocked down both Cdc42 and Rac1. The KD of both Cdc42 and Rac1 in PC12 cells by shRNAs resulted in a significant inhibition of K^+-evoked DA release from PC12 cells (Fig. 8*B*).

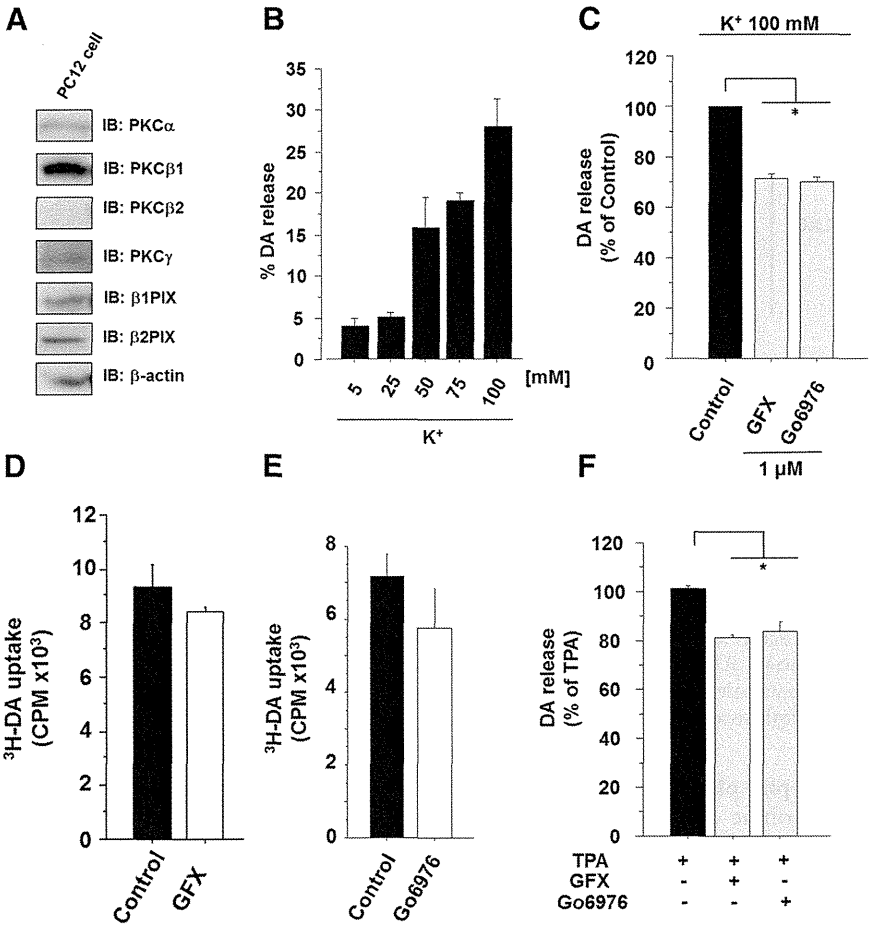

Figure 6. cPKC positively regulates K^+-stimulated DA release. ***A***, cPKCs and βPIX are expressed in PC12 cells. PC12 cell lysates were analyzed with immunoblotting with anti-PKCα, β1, β2, γ, and βPIX antibodies. ***B***, DA release in PC12 cells was measured with various K^+ concentrations. The results are expressed as mean ± SEM ($n = 3$). ***C***, Amounts of DA release that were stimulated in response to 100 mM K^+ with 1 μM GFX or 1 μM Gö6976 were measured in PC12 cells ($n = 3$; $^*p < 0.05$, unpaired *t* test). DA release levels were normalized to the levels released in response to 100 mM K^+, which were set to 100%. The results are expressed as mean ± SEM ($n = 3$–5). ***D***, ***E***, Uptake of ^{3}H-DA into PC12 cells with or without GFX and Gö6976 were measured. The results are expressed as mean ± SEM ($n = 3$). ***F***, TPA stimulated DA release in PC12 cells. DA release in PC12 cells was measured with 1 μM TPA in the absence or presence of 1 μM GFX. DA release levels were normalized to that of 1 μM TPA stimulation, which was set to 100%. The results are expressed as mean ± SEM ($n = 3$, $^*p < 0.01$, unpaired *t* test).

Discussion

In this study, we revealed that AS/AGU rats did not express full-length PKCγ or the truncated form of PKCγ, indicating that a loss, and not a gain, of function is the cause of the parkinsonian symptoms exhibited by AS/AGU rats. In agreement with these findings, we demonstrated decreased DA release stimulated by high levels of K^+ and METH in the striatum. It is noteworthy that altered DA release is the predominant characteristic of parkinsonian symptoms in PKCγ KO mice rather than loss of DAergic neurons in the SNpc. We propose that PKCγ KO animals are useful models for the study of parkinsonian syndrome because PKCγ KO mice and AS/AGU rats have damage not only in the DAergic system, but also in the serotonergic system (Al-Fayez et al., 2005), as has been observed in patients with sporadic Parkinson's disease. Furthermore, the use of the PKCγ KO mouse model has an advantage because it is possible to perform gene manipulations in them, such as PKCγ rescue, compared with the AS/AGU rats.

Although it is generally accepted that DA release in the striatum induced by high K^+ levels is mediated by exocytosis and not by DAT, PKC was reported to induce DAT endocytosis (Daniels and Amara, 1999), which, by altering DA reuptake, can change the amplitude of K^+-induced DA release as measured by microdialysis. We have ruled out this possibility because DAT activity was instead decreased in PKCγ KO mice (Fig. 1*F*). Moreover, ^{3}H-DA uptake does not differ between the control and PKC inhibitors in PC12 cells (Fig. 6*D*,*E*). These results suggested that the reduced K^+-induced DA release was not through the change of the DAT endocytosis by the PKCγ KO. There are also reports that activation of PKC induces DAT-mediated DA reverse transport (Kantor and Gnegy, 1998; Cowell et al., 2000). Although

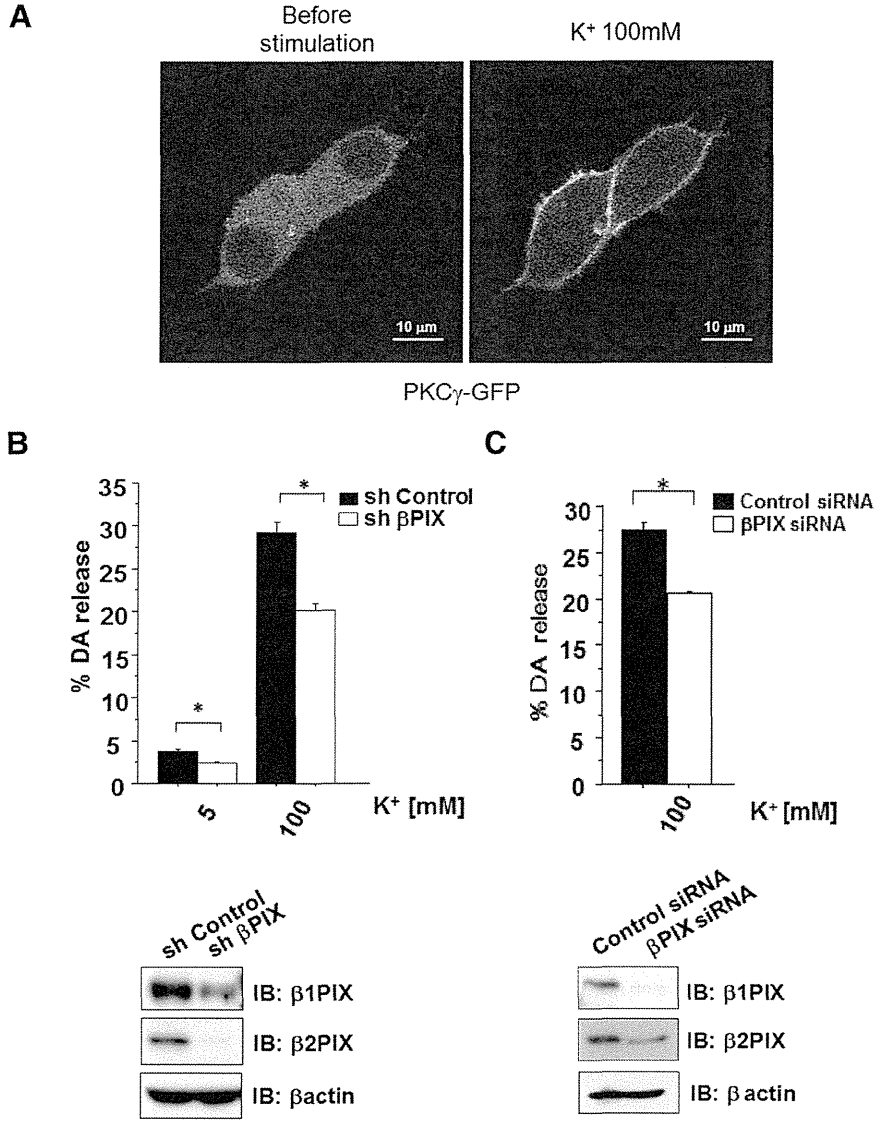

Figure 7. βPIX positively regulates K^+-stimulated DA release. ***A***, PKCγ was activated by high K^+ level stimulation in PC12 cells. Activation of PKCγ by K^+ stimulation was examined by monitoring the translocation of GFP-tagged PKCγ in PC12 cells. ***B***, DA release was measured in PC12 cells that were transfected with shRNA for βPIX and sh Control, which was used as a negative control. The results are expressed as mean ± SEM ($n = 6$, $^*p < 0.01$, *unpaired t* test). ***C***, DA release was measured in PC12 cells transfected with siRNA for βPIX. The expression of siRNAs for βPIX in PC12 cells and lysate was analyzed by immunoblot analyses with anti-βPIX antibodies. The results are expressed as mean ± SEM ($n = 5$, $^*p < 0.01$, unpaired *t* test).

these studies focused more on PKCβ than on PKCγ, our study showed that PKCγ also play important roles for DAT-mediated DA reverse transport (Fig. 1*F*), suggesting that PKCγ play roles for both K^+-mediated DA release and DAT-mediated DA reverse transport. Therefore, PKCγ KO resulted in decreased DAT activity, including uptaking DA and DA reverse transport through DAT. The decreased level of K^+-induced DA release in PKCγ KO mice is probably underestimated: DA release may be more significantly decreased when the disordered DAT activity is normalized.

We identified 10 phosphoproteins that were decreased in PKCγ KO mice under the hypothesis that decreased levels of phosphorylated substrates of PKCγ in the nigrostriatal system lead to impairments in DA release. Our results indicated that βPIX was one of the pivotal targets of PKCγ or cPKC in enhancing Ca^{2+}-evoked DA release based on the following several lines of evidence: (1) PKCγ phosphorylated βPIX *in vitro*, in cells, and *in vivo*; (2) Ser583 of βPIX was phosphorylated by PKCγ both *in vitro* and in cells, whereas Ser340 was phosphorylated by cPKC only in cells, suggesting that cPKC indirectly phosphorylated Ser340; (3) cPKC inhibitors and the KD of endogenous βPIX also suppressed the DA release from PC12 cells, suggesting that both PKCγ or cPKC and βPIX play pivotal roles in Ca^{2+}-evoked DA release from DAergic neurons; and (4) WT β2PIX, but not Ser340Ala or Ser583Ala, rescued the decreased DA release from PC12 cells by sh369 for βPIX, suggesting that both phosphorylation sites are necessary for regulating DA release. Why does PKCγ KO cause the parkinsonian syndrome phenotype, even when other cPKCs are expressed in PKCγ KO animals? Although the substrate specificity of each PKC subtype appears to be low *in vitro*, there have been several confirmatory reports of subtype-specific functions of cPKC under physiological conditions (Uchino et al., 2004; Ueyama et al., 2004; Al-Fayez et al., 2005; Kawasaki et al., 2010; Sakuma et al., 2012). Our data suggest that PKCγ has important roles in DA release in mice.

In neurons, Ca^{2+} entry triggers exocytosis, suggesting that certain Ca^{2+} sensors may be necessary for Ca^{2+}-dependent exocytosis. Candidates for Ca^{2+} sensors include molecules that possess EF hand motifs or C2 domains, which were first defined in cPKC, and annexin family proteins, as has been reported previously (Burgoyne and Morgan, 1998). PKC has been reported to modify exocytosis in the steps both before and after docking to the plasma membrane through the following mechanisms: (1) increased vesicle recruitment into the readily releasable pool (Gillis et al., 1996; Stevens and Sullivan, 1998), (2) acceleration of fusion pore expansion (Scepek et al., 1998), and (3) changes in the kinetics of exocytosis (Graham et al., 2002). However, βPIX is related to the exocytosis step after docking (Momboisse et al., 2009; Momboisse et al., 2010). The cPKC-βPIX- Cdc42/Rac1 axis possibly has important roles in DA release in the step after docking through the βPIX phosphorylation by cPKC.

How can βPIX regulate DA release through the phosphorylation at Ser340 or Ser583? Previous reports have revealed that βPIX phosphorylation results in βPIX translocation to the membrane and the subsequent activation of Rac1 and/or Cdc42. In PC12 cells, basic fibroblast growth factor induces the phosphorylation of βPIX at Ser525 and Thr526, resulting in neurite outgrowth by the activation of Rac1 through the translocation of the βPIX complex at neuronal growth cones (Shin et al., 2002; Shin et al., 2006). In human mesangial cells, endothelin-1 and cAMP inducers cause the PKA-dependent phosphorylation of βPIX at Ser516 and Thr526, resulting in cytoskeletal rearrangement by

the activation of Cdc42 through βPIX translocation (Chahdi et al., 2005). Therefore, βPIX may be differently phosphorylated in response to various stimuli and this may result in its stimulus-dependent specific targeting and Cdc42/Rac1 activation at the targeted sites. We have demonstrated for the first time that Ser583 is a PKCγ or cPKC phosphorylation site. Ser583 and the previously reported sites Ser516, Ser525, and Thr526 are all located in the C-terminal domain of βPIX and may have similar functions for the translocation and subsequent activation of Cdc42/Rac1. Phosphorylation at Ser340 is located in the PH domain, which interacts with phosphatidylinositol lipids within biological membranes (Wang and Shaw, 1995) and may also play important roles in the membrane targeting of βPIX. In fact, the PH domain has been reported to interact with PKC (Yao et al., 1994) and Cdc42 (Rossman et al., 2002) and it has been implicated in the regulation of the GEF activity of SOS (Ras-GEF; Karlovich et al., 1995) and p140Ras-GRF (Ras and Rac GEF; Buchsbaum et al., 1996). Therefore, through PH-domain-mediated membrane targeting and interaction, the cPKC-βPIX-Cdc42/Rac1 axis may act at specific membranes (Chen et al., 1997; Falasca et al., 1998; Maffucci and Falasca, 2001). Downstream of the βPIX phosphorylation, we speculate that Cdc42/Rac1 are the targets of phosphorylated βPIX, as suggested in previous studies (Shin et al., 2002; Shin et al., 2004; Chahdi et al., 2005; Shin et al., 2006). Although we have not proved a direct relationship between phosphorylated βPIX and Cdc42/Rac1, we speculate that βPIX phosphorylated by PKCγ regulates Cdc42/Rac1 functions based on our data that the double KD of Cdc42 and Rac1 resulted in decreased DA release (Fig. 8*B*).

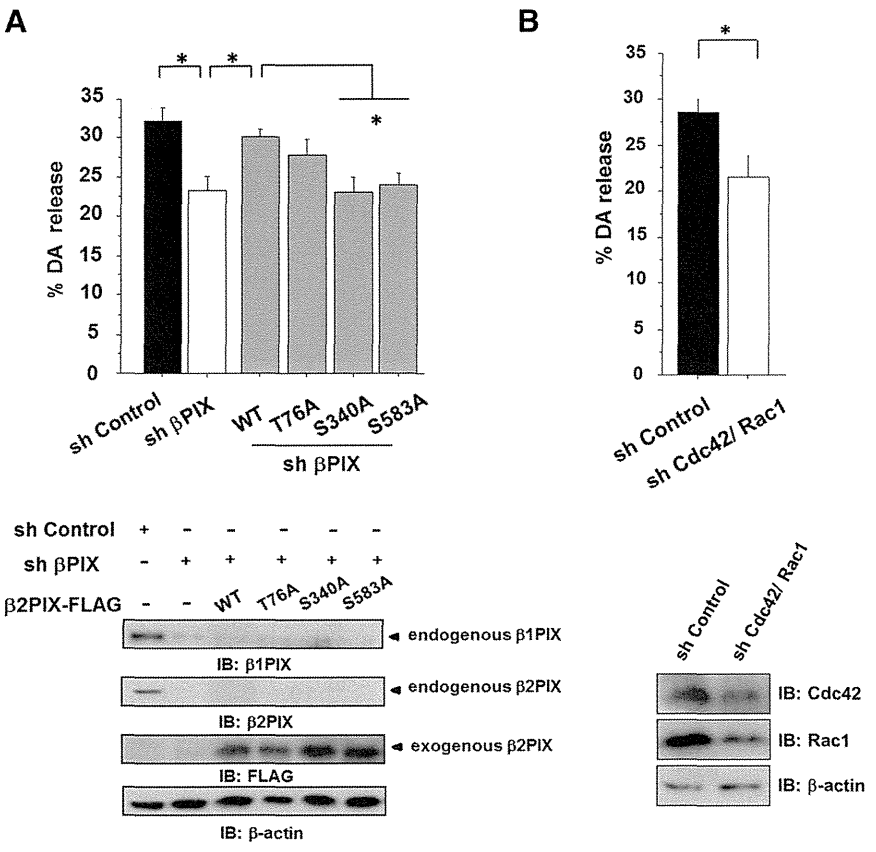

Figure 8. Phosphorylation of β2 PIX at Ser340 and Ser583 promotes DA release. ***A***, DA release was measured in PC12 cells that were transfected with shβPIX and β2PIX (WT and Ser-Ala mutants) with shRNA-resistant sequences. The levels of endogenous β1, β2PIX, and exogenous β2PIX were confirmed. Comparable levels of all ectopically expressed β2PIX proteins were confirmed by Western blot analyses. The results are expressed as mean ± SEM ($n = 3–6$, $^*p < 0.05$, one-way ANOVA with *post hoc* Dunnett's test). ***B***, DA release was measured in PC12 cells that were transfected with shRNA for both Cdc42 and Rac1 and sh Control, which was used as a negative control. The results are expressed as mean ± SEM ($n = 3$, $^*p < 0.01$, unpaired *t* test).

Although Ser340 is common to both β1PIX and β2PIX, Ser583 only exists in the unique C terminus of β2PIX, which is the neuron-dominant isoform (Koh et al., 2001) that emerged from and was conserved after *Xenopus laevis* (Fig. 9). Therefore, Ser583 phosphorylation by neuron-specific PKCγ may have important roles in the modulation of βPIX function in the highly developed CNS and highly elaborated function, including DA release. It is also of note that the reported phosphorylation sites at Ser340, Ser516, Ser525, and Thr526 are conserved through evolution. Although we detected the TPA-induced phosphorylation of β2PIX *in vivo* using the synaptosomal P2 fraction of PKCγ WT mice by pSer PKC motif Ab (Fig. 3*D*), we could not show clear TPA-induced phosphorylation at Ser340 and Ser583 in PKCγ WT using our site-specific phospho-Abs for pS340 and pS583, likely due to the sensitivity of anti-pS340 and pS583 Abs.

In the present study, we have demonstrated that PKCγ KO mice can be a useful model of parkinsonian syndrome. In addition, we found for the first time that DA release was positively regulated by the PKC-mediated direct phosphorylation of βPIX at Ser583 and indirect phosphorylation at Ser340. The phospho-

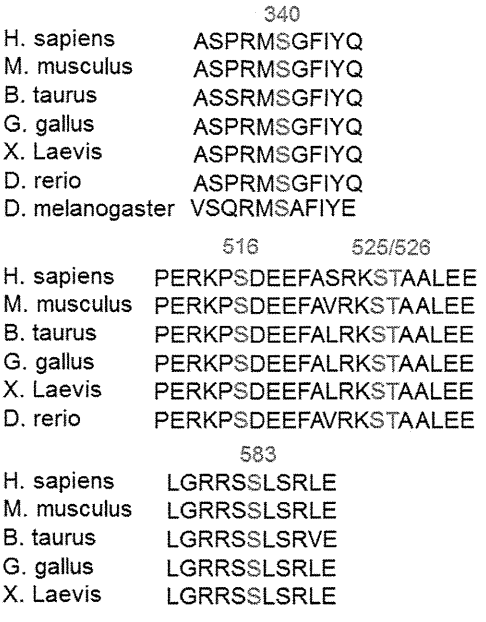

Figure 9. Schematic comparisons of Ser340 and Ser583 through evolution. Ser340 and Ser583 are evolutionally conserved in many species. It is noted that β2PIX emerged from *X. laevis*, although β1PIX is expressed in *Drosophila melanogaster*. Ser516, Ser525, and Thr526, as reported previously, are also conserved in many species.

rylational modulation of βPIX by PKCγ may be a potential therapeutic target for the treatment of parkinsonian syndrome.

References

Adachi N, Oyasu M, Taniguchi T, Yamaguchi Y, Takenaka R, Shirai Y, Saito N (2005) Immunocytochemical localization of a neuron-specific diacylglycerol kinase beta and gamma in the developing rat brain. Brain Res Mol Brain Res 139:288–299. CrossRef Medline

Ago Y, Araki R, Tanaka T, Sasaga A, Nishiyama S, Takuma K, Matsuda T (2013) Role of social encounter-induced activation of prefrontal serotonergic systems in the abnormal behaviors of isolation-reared mice. Neuropsychopharmacology 38:1535–1547. CrossRef Medline

Al-Fayez M, Russell D, Wayne Davies R, Shiels PG, Baker PJ, Payne AP (2005) Deficits in the mid-brain raphe nuclei and striatum of the AS/AGU rat, a protein kinase C-gamma mutant. Eur J Neurosci 22:2792–2798. CrossRef Medline

Audebert S, Navarro C, Nourry C, Chasserot-Golaz S, Lécine P, Bellaiche Y, Dupont JL, Premont RT, Sempéré C, Strub JM, Van Dorsselaer A, Vitale N, Borg JP (2004) Mammalian Scribble forms a tight complex with the betaPIX exchange factor. Curr Biol 14:987–995. CrossRef Medline

Barclay JW, Craig TJ, Fisher RJ, Ciufo LF, Evans GJ, Morgan A, Burgoyne RD (2003) Phosphorylation of Munc18 by protein kinase C regulates the kinetics of exocytosis. J Biol Chem 278:10538–10545. CrossRef Medline

Buchsbaum R, Telliez JB, Goonesekera S, Feig LA (1996) The N-terminal pleckstrin, coiled-coil, and IQ domains of the exchange factor Ras-GRF act cooperatively to facilitate activation by calcium. Mol Cell Biol 16:4888–4896. Medline

Burgoyne RD, Morgan A (1998) Calcium sensors in regulated exocytosis. Cell Calcium 24:367–376. CrossRef Medline

Campbell JM, Payne AP, Gilmore DP, Byrne JE, Russell D, McGadey J, Clarke DJ, Davies RW, Sutcliffe RG (1996) Neostriatal dopamine depletion and locomotor abnormalities due to the Albino Swiss rat agu mutation. Neurosci Lett 213:173–176. Medline

Chahdi A, Sorokin A (2008) Protein kinase A-dependent phosphorylation modulates beta1Pix guanine nucleotide exchange factor activity through 14–3-3beta binding. Mol Cell Biol 28:1679–1687. CrossRef Medline

Chahdi A, Miller B, Sorokin A (2005) Endothelin 1 induces beta 1Pix translocation and Cdc42 activation via protein kinase A-dependent pathway. J Biol Chem 280:578–584. CrossRef Medline

Chefer VI, Czyzyk T, Bolan EA, Moron J, Pintar JE, Shippenberg TS (2005) Endogenous kappa-opioid receptor systems regulate mesoaccumbal dopamine dynamics and vulnerability to cocaine. J Neurosci 25:5029–5037. CrossRef Medline

Chen RH, Corbalan-Garcia S, Bar-Sagi D (1997) The role of the PH domain in the signal-dependent membrane targeting of Sos. EMBO J 16:1351–1359. CrossRef Medline

Cowell RM, Kantor L, Hewlett GH, Frey KA, Gnegy ME (2000) Dopamine transporter antagonists block phorbol ester-induced dopamine release and dopamine transporter phosphorylation in striatal synaptosomes. Eur J Pharmacol 389:59–65. CrossRef Medline

Craig NJ, Durán Alonso MB, Hawker KL, Shiels P, Glencorse TA, Campbell JM, Bennett NK, Canham M, Donald D, Gardiner M, Gilmore DP, MacDonald RJ, Maitland K, McCallion AS, Russell D, Payne AP, Sutcliffe RG, Davies RW (2001) A candidate gene for human neurodegenerative disorders: a rat PKC gamma mutation causes a parkinsonian syndrome. Nat Neurosci 4:1061–1062. CrossRef Medline

Daniels GM, Amara SG (1999) Regulated trafficking of the human dopamine transporter: clathrin-mediated internalization and lysosomal degradation in response to phorbol esters. J Biol Chem 274:35794–35801. CrossRef Medline

Ding YQ, Xiang CX, Chen ZF (2005) Generation and characterization of the PKC gamma-Cre mouse line. Genesis 43:28–33. CrossRef Medline

Falasca M, Logan SK, Lehto VP, Baccante G, Lemmon MA, Schlessinger J (1998) Activation of phospholipase C gamma by PI 3-kinase-induced PH domain-mediated membrane targeting. EMBO J 17:414–422. CrossRef Medline

Feng Q, Baird D, Peng X, Wang J, Ly T, Guan JL, Cerione RA (2006) Cool-1 functions as an essential regulatory node for EGF receptor- and Src-mediated cell growth. Nat Cell Biol 8:945–956. CrossRef Medline

Franklin KBJ, Paxinos G (1997) The mouse brain in stereotaxic coordinates. San Diego: Academic.

Gillis KD, Mossner R, Neher E (1996) Protein kinase C enhances exocytosis from chromaffin cells by increasing the size of the readily releasable pool of secretory granules. Neuron 16:1209–1220. CrossRef Medline

Graham ME, O'Callaghan DW, McMahon HT, Burgoyne RD (2002) Dynamin-dependent and dynamin-independent processes contribute to the regulation of single vesicle release kinetics and quantal size. Proc Natl Acad Sci U S A 99:7124–7129. CrossRef Medline

Hewett J, Johanson P, Sharma N, Standaert D, Balcioglu A (2010) Function of dopamine transporter is compromised in DYT1 transgenic animal model in vivo. J Neurochem 113:228–235. CrossRef Medline

Hilfiker S, Pieribone VA, Nordstedt C, Greengard P, Czernik AJ (1999) Regulation of synaptotagmin I phosphorylation by multiple protein kinases. J Neurochem 73:921–932. CrossRef Medline

Iwasaki S, Kataoka M, Sekiguchi M, Shimazaki Y, Sato K, Takahashi M (2000) Two distinct mechanisms underlie the stimulation of neurotransmitter release by phorbol esters in clonal rat pheochromocytoma PC12 cells. J Biochem 128:407–414. CrossRef Medline

Justice JB Jr (1993) Quantitative microdialysis of neurotransmitters. J Neurosci Methods 48:263–276. CrossRef Medline

Kantor L, Gnegy ME (1998) Protein kinase C inhibitors block amphetamine-mediated dopamine release in rat striatal slices. J Pharmacol Exp Ther 284:592–598. Medline

Karlovich CA, Bonfini L, McCollam L, Rogge RD, Daga A, Czech MP, Banerjee U (1995) In vivo functional analysis of the Ras exchange factor son of sevenless. Science 268:576–579. CrossRef Medline

Kawasaki T, Ishihara K, Ago Y, Nakamura S, Itoh S, Baba A, Matsuda T (2006) Protective effect of the radical scavenger edaravone against methamphetamine-induced dopaminergic neurotoxicity in mouse striatum. Eur J Pharmacol 542:92–99. CrossRef Medline

Kawasaki T, Ishihara K, Ago Y, Baba A, Matsuda T (2007) Edaravone (3-methyl-1-phenyl-2-pyrazolin-5-one), a radical scavenger, prevents 1-methyl-4-phenyl-1,2,3,6-tetrahydropyridine-induced neurotoxicity in the substantia nigra but not the striatum. J Pharmacol Exp Ther 322:274–281. CrossRef Medline

Kawasaki T, Ueyama T, Lange I, Feske S, Saito N (2010) Protein kinase C-induced phosphorylation of Orai1 regulates the intracellular Ca^{2+} level via the store-operated Ca^{2+} channel. J Biol Chem 285:25720–25730. CrossRef Medline

Koda K, Ago Y, Cong Y, Kita Y, Takuma K, Matsuda T (2010) Effects of acute and chronic administration of atomoxetine and methylphenidate on extracellular levels of noradrenaline, dopamine and serotonin in the prefrontal cortex and striatum of mice. J Neurochem 114:259–270. CrossRef Medline

Koh CG, Manser E, Zhao ZS, Ng CP, Lim L (2001) Beta1PIX, the PAK-interacting exchange factor, requires localization via a coiled-coil region to promote microvillus-like structures and membrane ruffles. J Cell Sci 114:4239–4251. Medline

Kose A, Ito A, Saito N, Tanaka C (1990) Electron microscopic localization of gamma- and beta II-subspecies of protein kinase C in rat hippocampus. Brain Res 518:209–217. CrossRef Medline

Kyono Y, Sugiyama N, Imami K, Tomita M, Ishihama Y (2008) Successive and selective release of phosphorylated peptides captured by hydroxy acid-modified metal oxide chromatography. J Proteome Res 7:4585–4593. CrossRef Medline

Maffucci T, Falasca M (2001) Specificity in pleckstrin homology (PH) domain membrane targeting: a role for a phosphoinositide-protein cooperative mechanism. FEBS Lett 506:173–179. CrossRef Medline

Matsubara T, Ikeda M, Kiso Y, Sakuma M, Yoshino K, Sakane F, Merida I, Saito N, Shirai Y (2012) c-Abl tyrosine kinase regulates serum-induced nuclear export of diacylglycerol kinase α by phosphorylation at Tyr-218. J Biol Chem 287:5507–5517. CrossRef Medline

Mayhew MW, Jeffery ED, Sherman NE, Nelson K, Polefrone JM, Pratt SJ, Shabanowitz J, Parsons JT, Fox JW, Hunt DF, Horwitz AF (2007) Identification of phosphorylation sites in betaPIX and PAK1. J Cell Sci 120:3911–3918. CrossRef Medline

Momboisse F, Lonchamp E, Calco V, Ceridono M, Vitale N, Bader MF, Gasman S (2009) betaPIX-activated Rac1 stimulates the activation of phospholipase D, which is associated with exocytosis in neuroendocrine cells. J Cell Sci 122:798–806. CrossRef Medline

Momboisse F, Ory S, Ceridono M, Calco V, Vitale N, Bader MF, Gasman S (2010) The Rho guanine nucleotide exchange factors Intersectin 1L and β-Pix control calcium-regulated exocytosis in neuroendocrine PC12 cells. Cell Mol Neurobiol 30:1327–1333. CrossRef Medline

Murray D, Honig B (2002) Electrostatic control of the membrane targeting of C2 domains. Mol Cell 9:145–154. CrossRef Medline

Nishizuka Y (1988) The molecular heterogeneity of protein kinase C and its implications for cellular regulation. Nature 334:661–665. CrossRef Medline

Nishizuka Y (1992) Intracellular signaling by hydrolysis of phospholipids and activation of protein kinase C. Science 258:607–614. CrossRef Medline

Ota T, Suzuki Y, Nishikawa T, Otsuki T, Sugiyama T, Irie R, Wakamatsu A, Hayashi K, Sato H, Nagai K, Kimura K, Makita H, Sekine M, Obayashi M, Nishi T, Shibahara T, Tanaka T, Ishii S, Yamamoto J, Saito K, et al. (2004) Complete sequencing and characterization of 21,243 full-length human cDNAs. Nat Genet 36:40–45. CrossRef Medline

Payne AP, Campbell JM, Russell D, Favor G, Sutcliffe RG, Bennett NK, Davies RW, Stone TW (2000) The AS/AGU rat: a spontaneous model of disruption and degeneration in the nigrostriatal dopaminergic system. J Anat 196:629–633. CrossRef Medline

Rossman KL, Worthylake DK, Snyder JT, Siderovski DP, Campbell SL, Sondek J (2002) A crystallographic view of interactions between Dbs and Cdc42: PH domain-assisted guanine nucleotide exchange. EMBO J 21:1315–1326. CrossRef Medline

Saito H, Oda Y, Sato T, Kuromitsu J, Ishihama Y (2006) Multiplexed two-dimensional liquid chromatography for MALDI and nanoelectrospray ionization mass spectrometry in proteomics. J Proteome Res 5:1803–1807. CrossRef Medline

Saito N, Shirai Y (2002) Protein kinase C gamma (PKC gamma): function of neuron specific isotype. J Biochem 132:683–687. CrossRef Medline

Sakuma M, Shirai Y, Yoshino K, Kuramasu M, Nakamura T, Yanagita T, Mizuno K, Hide I, Nakata Y, Saito N (2012) Novel PKCα-mediated phosphorylation site(s) on cofilin and their potential role in terminating histamine release. Mol Biol Cell 23:3707–3721. CrossRef Medline

Scepek S, Coorssen JR, Lindau M (1998) Fusion pore expansion in horse eosinophils is modulated by Ca^{2+} and protein kinase C via distinct mechanisms. EMBO J 17:4340–4345. CrossRef Medline

Seki T, Adachi N, Ono Y, Mochizuki H, Hiramoto K, Amano T, Matsubayashi H, Matsumoto M, Kawakami H, Saito N, Sakai N (2005) Mutant protein kinase Cgamma found in spinocerebellar ataxia type 14 is susceptible to aggregation and causes cell death. J Biol Chem 280:29096–29106. CrossRef Medline

Shin EY, Shin KS, Lee CS, Woo KN, Quan SH, Soung NK, Kim YG, Cha CI, Kim SR, Park D, Bokoch GM, Kim EG (2002) Phosphorylation of p85 beta PIX, a Rac/Cdc42-specific guanine nucleotide exchange factor, via the Ras/ERK/PAK2 pathway is required for basic fibroblast growth factor-induced neurite outgrowth. J Biol Chem 277:44417–44430. CrossRef Medline

Shin EY, Woo KN, Lee CS, Koo SH, Kim YG, Kim WJ, Bae CD, Chang SI, Kim EG (2004) Basic fibroblast growth factor stimulates activation of Rac1 through a p85 betaPIX phosphorylation-dependent pathway. J Biol Chem 279:1994–2004. CrossRef Medline

Shin EY, Lee CS, Cho TG, Kim YG, Song S, Juhnn YS, Park SC, Manser E, Kim EG (2006) betaPak-interacting exchange factor-mediated Rac1 activation requires smgGDS guanine nucleotide exchange factor in basic fibroblast growth factor-induced neurite outgrowth. J Biol Chem 281:35954–35964. CrossRef Medline

Stevens CF, Sullivan JM (1998) Regulation of the readily releasable vesicle pool by protein kinase C. Neuron 21:885–893. CrossRef Medline

ten Klooster JP, Jaffer ZM, Chernoff J, Hordijk PL (2006) Targeting and activation of Rac1 are mediated by the exchange factor beta-Pix. J Cell Biol 172:759–769. CrossRef Medline

Uchino M, Sakai N, Kashiwagi K, Shirai Y, Shinohara Y, Hirose K, Iino M, Yamamura T, Saito N (2004) Isoform-specific phosphorylation of metabotropic glutamate receptor 5 by protein kinase C (PKC) blocks Ca^{2+} oscillation and oscillatory translocation of Ca^{2+}-dependent PKC. J Biol Chem 279:2254–2261. CrossRef Medline

Ueyama T, Lennartz MR, Noda Y, Kobayashi T, Shirai Y, Rikitake K, Yamasaki T, Hayashi S, Sakai N, Seguchi H, Sawada M, Sumimoto H, Saito N (2004) Superoxide production at phagosomal cup/phagosome through βI protein kinase C during FcγR-mediated phagocytosis in microglia. J Immunol 173:4582–4589. CrossRef Medline

Ueyama T, Geiszt M, Leto TL (2006) Involvement of Rac1 in activation of multicomponent Nox1- and Nox3-based NADPH oxidases. Mol Cell Biol 26:2160–2174. CrossRef Medline

Ueyama T, Sakaguchi H, Nakamura T, Goto A, Morioka S, Shimizu A, Nakao K, Hishikawa Y, Ninoyu Y, Kassai H, Suetsugu S, Koji T, Fritzsch B, Yonemura S, Hisa Y, Matsuda M, Aiba A, Saito N (2014) Maintenance of stereocilia and apical junctional complexes by Cdc42 in cochlear hair cells. J Cell Sci 127:2040–2052. CrossRef Medline

Wang DS, Shaw G (1995) The association of the C-terminal region of beta I sigma II spectrin to brain membranes is mediated by a PH domain, does not require membrane proteins, and coincides with a inositol-1,4,5 triphosphate binding site. Biochem Biophys Res Commun 217:608–615. CrossRef Medline

Wu WC, Walaas SI, Nairn AC, Greengard P (1982) Calcium/phospholipid regulates phosphorylation of a Mr "87k" substrate protein in brain synaptosomes. Proc Natl Acad Sci U S A 79:5249–5253. CrossRef Medline

Yao L, Kawakami Y, Kawakami T (1994) The pleckstrin homology domain of Bruton tyrosine kinase interacts with protein kinase C. Proc Natl Acad Sci U S A 91:9175–9179. CrossRef Medline

PLOS ONE

Contribution of Dysferlin Deficiency to Skeletal Muscle Pathology in Asymptomatic and Severe Dystroglycanopathy Models: Generation of a New Model for Fukuyama Congenital Muscular Dystrophy

Motoi Kanagawa[1¶], Zhongpeng Lu[1¶], Chiyomi Ito[1], Chie Matsuda[2], Katsuya Miyake[3], Tatsushi Toda[1]*

1 Division of Neurology/Molecular Brain Science, Kobe University Graduate School of Medicine, Kobe, Japan, **2** Biomedical Research Institute, National Institute of Advanced Industrial Science and Technology, Tsukuba, Japan, **3** Department of Histology and Cell Biology, School of Medicine, Kagawa University, Ikenobe, Miki, Kagawa, Japan

Abstract

Defects in dystroglycan glycosylation are associated with a group of muscular dystrophies, termed dystroglycanopathies, that include Fukuyama congenital muscular dystrophy (FCMD). It is widely believed that abnormal glycosylation of dystroglycan leads to disease-causing membrane fragility. We previously generated knock-in mice carrying a founder retrotransposal insertion in *fukutin*, the gene responsible for FCMD, but these mice did not develop muscular dystrophy, which hindered exploring therapeutic strategies. We hypothesized that dysferlin functions may contribute to muscle cell viability in the knock-in mice; however, pathological interactions between glycosylation abnormalities and dysferlin defects remain unexplored. To investigate contributions of dysferlin deficiency to the pathology of dystroglycanopathy, we have crossed dysferlin-deficient *dysferlin*$^{sjl/sjl}$ mice to the fukutin-knock-in *fukutin*$^{Hp/-}$ and Large-deficient *Large*$^{myd/myd}$ mice, which are phenotypically distinct models of dystroglycanopathy. The *fukutin*$^{Hp/-}$ mice do not show a dystrophic phenotype; however, (*dysferlin*$^{sjl/sjl}$: *fukutin*$^{Hp/-}$) mice showed a deteriorated phenotype compared with (*dysferlin*$^{sjl/sjl}$: *fukutin*$^{Hp/+}$) mice. These data indicate that the absence of functional dysferlin in the asymptomatic *fukutin*$^{Hp/-}$ mice triggers disease manifestation and aggravates the dystrophic phenotype. A series of pathological analyses using double mutant mice for Large and dysferlin indicate that the protective effects of dysferlin appear diminished when the dystrophic pathology is severe and also may depend on the amount of dysferlin proteins. Together, our results show that dysferlin exerts protective effects on the *fukutin*$^{Hp/-}$ FCMD mouse model, and the (*dysferlin*$^{sjl/sjl}$: *fukutin*$^{Hp/-}$) mice will be useful as a novel model for a recently proposed antisense oligonucleotide therapy for FCMD.

Citation: Kanagawa M, Lu Z, Ito C, Matsuda C, Miyake K, et al. (2014) Contribution of Dysferlin Deficiency to Skeletal Muscle Pathology in Asymptomatic and Severe Dystroglycanopathy Models: Generation of a New Model for Fukuyama Congenital Muscular Dystrophy. PLoS ONE 9(9): e106721. doi:10.1371/journal.pone.0106721

Editor: Diego Fraidenraich, Rutgers University -New Jersey Medical School, United States of America

Received March 31, 2014; **Accepted** August 1, 2014; **Published** September 8, 2014

Data Availability: The authors confirm that all data underlying the findings are fully available without restriction. All relevant data are within the paper.

Funding: This work was supported by the Ministry of Health, Labor and Welfare of Japan [Intramural Research Grant for Neurological and Psychiatric Disorders of National Center of Neurology and Psychiatry (23B-5)] to T.T. and C.M. (http://www.mhlw.go.jp/english/index.html); the Ministry of Education, Culture, Sports, Science and Technology of Japan [a Grant-in-Aid for Scientific Research (A) 23249049 to T.T.; a Grant-in-Aid for Young Scientists (A) 24687017 to M.K.; a Grant-in-Aid for Exploratory Research (23659454 to M.K.); and a Grant-in-Aid for Scientific Research on Innovative Areas (Deciphering sugar chain-based signals regulating integrative neuronal functions) 24110508 to M.K.] (http://www.mext.go.jp/english/); a Senri Life Science Foundation grant to M.K. (http://www.senri-life.or.jp/); a Takeda Science Foundation grant to M.K. (http://www.takeda-sci.or.jp/); and a Naito Foundation grant to M.K. (https://www.naito-f.or.jp/jp/index.php). The funders had no role in study design, data collection and analysis, decision to publish, or preparation of the manuscript.

Competing Interests: The authors have declared that no competing interests exist.

* Email: toda@med.kobe-u.ac.jp

¶ These authors are joint first authors on this work.

Introduction

Muscular dystrophies are a heterogeneous group of genetic disorders characterized by the progressive loss of muscle strength and integrity. Several lines of evidence have established that the structural linkage between the muscle extracellular matrix and the cytoskeleton is essential in preventing the progression of muscular dystrophy [1]. The dystrophin-glycoprotein complex (DGC) forms the structural linkage, and mutations in components of this complex cause several forms of muscular dystrophy, including Duchenne and limb-girdle muscular dystrophies (LGMDs) [2]. Within the DGC, α- and β-dystroglycans (DG) act as a molecular bridge between the extracellular matrix and the cytoskeleton. α-DG is a highly glycosylated extracellular subunit that functions as a receptor for extracellular matrix proteins such as laminins. *O*-mannosyl glycosylation and a novel phosphodiester-linked modification of *O*-mannose, termed post-phosphoryl modification, are necessary for α-DG to serve as a functional laminin receptor [3,4]. α-DG is anchored on the plasma membrane through non-covalent interaction with a transmembrane-type β-DG, which in turn binds to the dystrophin-actin cytoskeleton.

Fukuyama congenital muscular dystrophy (FCMD: MIM 253800) is an autosomal recessive disorder characterized by severe

muscular dystrophy, abnormal neuronal migration associated with mental retardation and, frequently, eye abnormalities [5]. We identified *fukutin*, the gene responsible for FCMD, and a 3-kb SINE-VNTR-*Alu* (SVA) retrotransposon insertion into the 3′ UTR of *fukutin* as the founder mutation in FCMD [6]. This insertion causes abnormal splicing that leads to the production of non-functional fukutin protein [7]. The introduction of antisense oligonucleotides that target the splice acceptor and splicing enhancers prevented the pathogenic abnormal splicing by SVA in the cells of FCMD patients as well as model mice that carry the retrotransposal insertion [7]. Point mutations in *fukutin* have been reported in patients both inside and outside Japan, and recent studies have revealed a broad clinical spectrum for fukutin-deficient muscular dystrophies [8]. In FCMD, α-DG is abnormally glycosylated, and its laminin-binding activity is decreased [3]. Several other forms of muscular dystrophy are caused by abnormal glycosylation of α-DG; collectively, these conditions are termed "dystroglycanopathies". More than 10 genes have been identified as causative genes in dystroglycanopathies [9–14], some of which encode products that possess enzyme activities involved in synthesizing *O*-mannosyl sugar chains on α-DG [15–18]. Fukutin, LARGE, and Fukutin-related protein (FKRP) participate in forming the post-phosphoryl moiety [4,19]. Overall, dystroglycanopathy gene products appear to be involved in *O*-mannosyl chain synthesis and post-phosphoryl modification; mutations in these pathways commonly result in abnormal glycosylation of α-DG and reduced ligand-binding activity, disrupting the DG-mediated linkage between the extracellular matrix and the cytoskeleton [2].

Defects in DGC components or α-DG glycosylation disrupt the linkage between the extracellular matrix and the cytoskeleton, thus rendering the sarcolemma more susceptible to contraction-induced damage. This is thought to trigger an increase in intracellular Ca^{2+} concentration, eventually leading to necrosis and myofiber degeneration. Myofibers possess an intrinsic mechanism for repair of damaged membranes, and dysferlin plays a pivotal role in the skeletal muscle membrane repair pathway. In humans, dysferlin deficiency leads to LGMD2B, Miyoshi myopathy or a distal myopathy with anterior tibial onset [20]. Dysferlin-deficient mice show defective membrane repair and also develop muscular dystrophy [21]. Several proteins are known to interact with dysferlin [20], and it is expected that these proteins also participate in membrane repair. For example, mitsugumin 53 (MG53, also known as TRIM72) has been implicated in vesicle trafficking to the damage site during the membrane repair process [22].

We previously described a new FCMD mouse model that carries the retrotransposal insertion in the mouse *fukutin* ortholog [23]. These knock-in mice exhibit hypoglycosylated α-DG but do not develop muscular dystrophy. Therefore, these mice are not suitable for testing effectiveness of the antisense oligonucleotide therapy for FCMD. Although skeletal muscle-selective fukutin conditional knock-out mice, namely MCK-fukutin-cKO and Myf5-fukutin-cKO, show dystrophic phenotype [24], they are not applicable for the examination of the antisense oligonucleotide therapy because they do not possess the retrotransposal insertion. We previously reported that the small amount of normally glycosylated α-DG remaining in the skeletal muscle of the knock-in mice prevents muscular dystrophy [23]. However, it is not clear whether this residual glycosylation alone is sufficient to maintain skeletal muscle membrane integrity. We hypothesized that dysferlin functions compensate for presumed membrane fragility caused by a reduced interaction between α-DG and laminin. Furthermore, the exact contribution of dysferlin and dysferlin-interacting proteins to the pathology of dystroglycanopathy is not known. To investigate this question, we crossed dysferlin-deficient mice with two distinct dystroglycanopathy mouse models and analyzed the resultant phenotypes. In addition, if the double mutant mice carrying the retrotransposal insertion show worse dystrophic phenotype than those of dysferlin mutant mice, they can be the first model for the novel antisense oligonucleotide therapy for FCMD.

Materials and Methods

Animals

Dysferlin-deficient SJL/J mice, a strain with a large deletion in the *Dysf* gene [25], were purchased from Charles River Japan. The transgenic mouse carrying a neo cassette disruption of one *fukutin* allele (*fukutin*$^{+/-}$) [26] and the transgenic knock-in homozygous mutant mouse carrying the retrotransposal insertion in the mouse *fukutin* ortholog (*fukutin*$^{Hp/Hp}$) have been described previously [23]. Genotyping for the *Dysf* mutant allele and the *fukutin* mutant allele was performed as described previously [23,25]. All animal procedures were approved by the Animal Care and Use Committee of Kobe University Graduate School of Medicine (P120202-R2) in accordance with guidelines of Ministry of Education, Culture, Sports, Science and Technology (MEXT) and Japan Society for the Promotion of Science (JSPS). The animals were housed in cages (2–4 mice per cage) with wood-chip bedding in an environmentally controlled room (25°C, 12 h light-dark cycle) and provided food and water *ad libitum* at the animal facility of Kobe University Graduate School of Medicine. Well-trained and skilled researchers and experimental technicians, who have knowledge of methods to prevent unnecessary excessive pain, handled the animals and carried out the experiments. Euthanization was done by cervical dislocation. At sacrifice, the muscles were harvested and snap-frozen in liquid nitrogen (for biochemistry) or in liquid-nitrogen-cooled isopentane (for immunofluorescence and histology). The number and ages of animals used in each experiment is indicated in Figure legends and graphs.

To generate double mutant mice for dysferlin and fukutin deficiency, we crossed dysferlin-deficient SJL/J mice [25] (*dysferlin*$^{sjl/sjl}$; SJL background) with two different lines of *fukutin* mutant mice. One is a transgenic mouse carrying a neo cassette disruption for a single *fukutin* allele (*fukutin*$^{+/-}$; 129-C57BL/6 background) [26] (Fig. 1A, line A). The other is a transgenic knock-in homozygous mutant mouse carrying the retrotransposal insertion in the mouse *fukutin* ortholog [23] (*fukutin*$^{Hp/Hp}$; 129-C57BL/6 background) (Fig. 1A, line B). Heterozygous F1 mice in both lines were intercrossed to obtain the following four genotypes (F2): (*dysferlin*$^{sjl/sjl}$: *fukutin*$^{+/-}$); (*dysferlin*$^{sjl/+}$: *fukutin*$^{+/-}$); (*dysferlin*$^{sjl/+}$: *fukutin*$^{Hp/Hp}$); and (*dysferlin*$^{sjl/sjl}$: *fukutin*$^{Hp/Hp}$). We further crossed (*dysferlin*$^{sjl/sjl}$: *fukutin*$^{+/-}$) with (*dysferlin*$^{sjl/+}$: *fukutin*$^{Hp/Hp}$) mice or (*dysferlin*$^{sjl/+}$: *fukutin*$^{+/-}$) with (*dysferlin*$^{sjl/sjl}$: *fukutin*$^{Hp/Hp}$) mice (Fig. 1A, highlighted with gray) to produce four genotypes (F3): (*dysferlin*$^{sjl/+}$: *fukutin*$^{Hp/+}$); (*dysferlin*$^{sjl/+}$: *fukutin*$^{Hp/-}$); (*dysferlin*$^{sjl/sjl}$: *fukutin*$^{Hp/+}$); and (*dysferlin*$^{sjl/sjl}$: *fukutin*$^{Hp/-}$). To generate double mutant mice for dysferlin and Large deficiency, we crossed dysferlin-deficient SJL/J mice (C57BL/6 backcross 7) with Large-deficient *Large*^{myd} mice (*Large*$^{myd/myd}$; C57BL/6 background) [27,28]. Heterozygous F1 mice were intercrossed and the following four genotypes were used for the analyses (F2): (*dysferlin*$^{sjl/+}$: *Large*$^{myd/+}$); (*dysferlin*$^{sjl/sjl}$: *Large*$^{myd/+}$); (*dysferlin*$^{sjl/+}$: *Large*$^{myd/myd}$); and (*dysferlin*$^{sjl/sjl}$: *Large*$^{myd/myd}$). For more effective breeding, we crossed (*dysferlin*$^{sjl/+}$: *Large*$^{myd/+}$) mice with (*dysferlin*$^{sjl/sjl}$: *Large*$^{myd/+}$) mice (Fig. 1B). (*Dysferlin*$^{+/+}$: *Large*$^{myd/myd}$) mice were obtained from

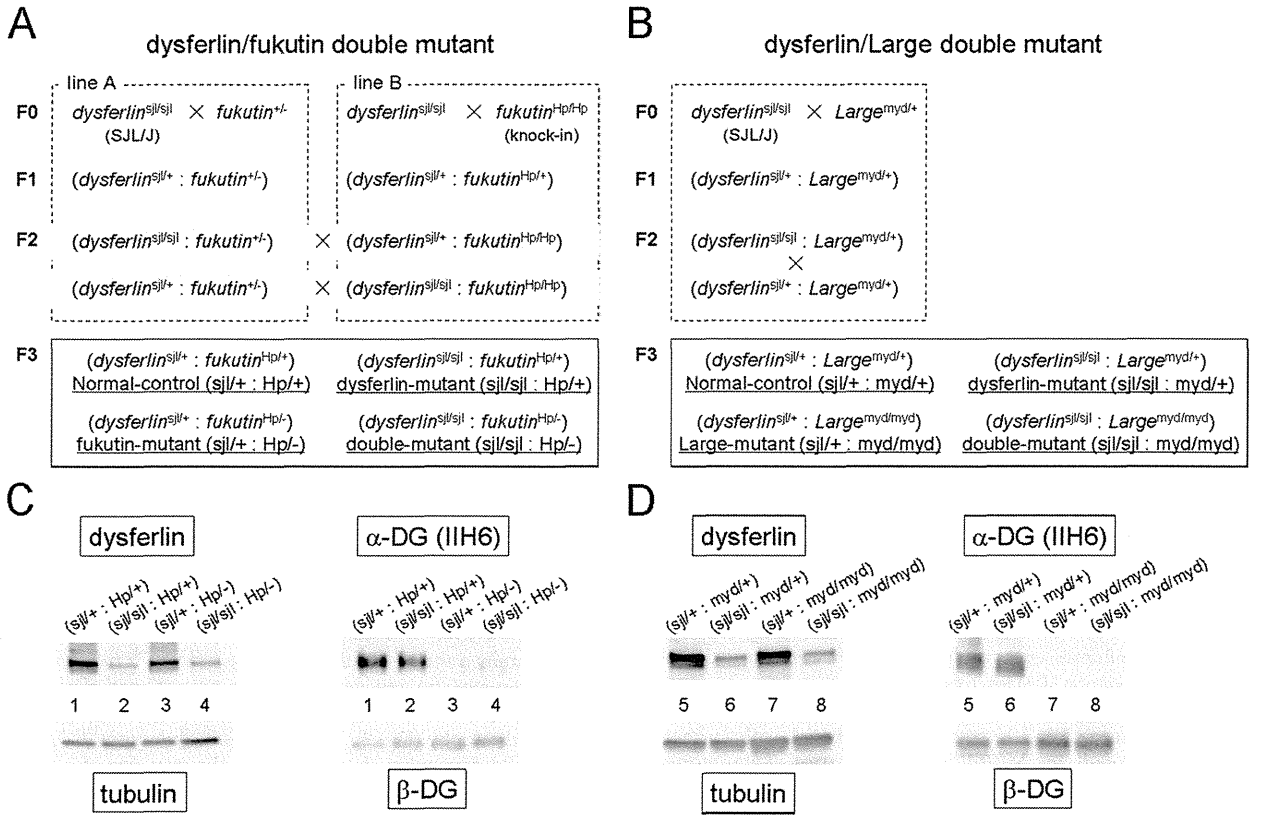

Figure 1. Generation of double-mutant mice exhibiting both abnormal α-DG glycosylation and reduced dysferlin expression. (A, B) Breeding strategy for the generation of double-mutant mice. sjl represents the *dysferlin* mutant allele, myd represents the *Large* mutant allele, and Hp represents the transgenic allele carrying the retrotransposal insertion in *fukutin*. Hp/+ represents a carrier with the insertion in *fukutin*. Hp/− represents a compound heterozygote carrying the insertion and a neo-disrupted allele. For the dysferlin/fukutin double mutant line, we used mice carrying *dysferlin*$^{sjl/+}$ and *fukutin*$^{Hp/+}$ as the normal control (*dysferlin*$^{sjl/+}$: *fukutin*$^{Hp/+}$); *dysferlin*$^{sjl/sjl}$ and *fukutin*$^{Hp/+}$ as the *dysferlin*-mutant (*dysferlin*$^{sjl/sjl}$: *fukutin*$^{Hp/+}$); *dysferlin*$^{sjl/+}$ and *fukutin*$^{Hp/-}$ as the *fukutin*-mutant (*dysferlin*$^{sjl/+}$: *fukutin*$^{Hp/-}$); and *dysferlin*$^{sjl/sjl}$ and *fukutin*$^{Hp/-}$ as the double-mutant (*dysferlin*$^{sjl/sjl}$: *fukutin*$^{Hp/-}$). For the dysferlin/Large double mutant line, we used mice carrying *dysferlin*$^{sjl/+}$ and *Large*$^{myd/+}$ as the normal control (*dysferlin*$^{sjl/+}$: *Large*$^{myd/+}$); *dysferlin*$^{sjl/sjl}$ and *Large*$^{myd/+}$ as the *dysferlin*-mutant (*dysferlin*$^{sjl/sjl}$: *Large*$^{myd/+}$); *dysferlin*$^{sjl/+}$ and *Large*$^{myd/myd}$ as the *Large*-mutant (*dysferlin*$^{sjl/+}$: *Large*$^{myd/myd}$); and *dysferlin*$^{sjl/sjl}$ and *Large*$^{myd/myd}$ as the double mutant (*dysferlin*$^{sjl/sjl}$: *Large*$^{myd/myd}$). (C, D) Abnormal α-DG glycosylation and reduced dysferlin protein expression. Solubilized skeletal muscle samples from each genotype were subjected to Western blot analysis for dysferlin protein expression (left panel). Tubulin was used as a loading control. The solubilized fractions were further enriched for DG by WGA-beads, and the DG-enriched fractions were subjected to Western blotting with the monoclonal IIH6 antibody, which recognizes glycosylated α-DG (right panel). β-DG was used as a loading control. The (*dysferlin*$^{sjl/+}$: *fukutin*$^{Hp/+}$), (*dysferlin*$^{sjl/sjl}$: *fukutin*$^{Hp/+}$), (*dysferlin*$^{sjl/+}$: *fukutin*$^{Hp/-}$), and (*dysferlin*$^{sjl/sjl}$: *fukutin*$^{Hp/-}$) mice are abbreviated as (sjl/+: Hp/+), (sjl/sjl: Hp/+), (sjl/+: Hp/−), and (sjl/sjl: Hp/−), respectively. The (*dysferlin*$^{sjl/+}$: *Large*$^{myd/+}$), (*dysferlin*$^{sjl/sjl}$: *Large*$^{myd/+}$), (*dysferlin*$^{sjl/+}$: *Large*$^{myd/myd}$), and (*dysferlin*$^{sjl/sjl}$: *Large*$^{myd/myd}$) mice are abbreviated as (sjl/+: myd/+), (sjl/sjl: myd/+), (sjl/+: myd/myd), and (sjl/sjl: myd/myd), respectively.
doi:10.1371/journal.pone.0106721.g001

the dysferlin/Large double mutant line and *Large*^{myd} mouse colonies.

Antibodies

Antibodies used in Western blotting and immunofluorescence were as follows: mouse monoclonal antibody 8D5 against β-DG (Novocastra); mouse monoclonal antibody IIH6 against α-DG (Millipore); affinity-purified goat polyclonal antibody against the α-DG core protein (AP-074G-C) [23]; mouse monoclonal antibody NCL-Hamlet against dysferlin (Novocastra); rat monoclonal antibody against mouse F4/80 (BioLegend); rabbit polyclonal antibody against collagen I (AbD serotec); rabbit polyclonal antibody against albumin (DAKO); mouse monoclonal antibody against caveolin-3 (BD Transduction Laboratories); rabbit polyclonal antibody against caveolin-3 (Abcam); and rabbit polyclonal antibody against Trim72 (MG53) (Abcam).

Protein preparation and Western blotting

DG was enriched from solubilized skeletal muscle as described previously [23]. Briefly, skeletal muscles were solubilized in Tris-buffered saline (TBS) containing 1% Triton X-100 and protease inhibitors (Nacalai). The solubilized fraction was incubated with wheat germ agglutinin (WGA)-agarose beads (Vector Laboratories) at 4°C for 16 h, and then DG was eluted with SDS-PAGE loading buffer. For detection of dysferlin and dysferlin-interacting proteins, RIPA buffer (1% NP-40, 0.5% DOC, and 0.1% SDS in TBS with protease inhibitors) was used for protein extraction from skeletal muscle. For this experiment, we used *fukutin*$^{Hp/-}$ mice and litter control *fukutin*$^{Hp/+}$ mice that were backcrossed to C57BL/6 mice more than 10 times. Protein concentration of the solubilized fractions was measured by Lowry methods, using BSA as a standard. Proteins were separated using 3–15% linear gradient SDS-gels. Gels were transferred to polyvinylidene fluoride

(PVDF) membrane (Millipore). Blots were probed with antibodies and then developed with horseradish peroxidase (HRP)-enhanced chemiluminescence (Supersignal West Pico, Pierce; or ECL Plus, GE Healthcare). Protein bands were detected using the LAS-4000 system (Fujifilm), and band intensities were quantified using Multi Gauge V3.2 software (Fujifilm). Statistical analysis was performed with a two-tailed unpaired t test. A p value of <0.05 was considered to be significant.

Histological and Immunofluorescence analysis

For H&E staining, cryosections (7 μm) were stained for 2 min in hematoxylin, 1 min in eosin, and then dehydrated with ethanol and xylenes. For Masson trichrome staining, sections were fixed with Bouin's solution (Sigma) for 1 hour at 60°C. The slides were incubated in solution A (5% trichloroacetic acid, 5% potassium dichromate) for 30 min, and then stained with Weigert's iron hematoxylin (Muto Chemical Co Ltd) for 15 min. After a rinse with 0.5% HCl in 70% ethanol and a subsequent rinse with warm water, the slides were incubated in solution B (0.5% phosphotungstic acid, 2.5% phosphomolybdic acid) for 1 min, and then stained with FUCHSIN-PONCEAU solution. The slides were washed with 1% acetic acid, incubated in 2.5% phosphomolybdic acid for 5 min, washed with 1% acetic acid, stained with aniline blue, washed with 1% acetic acid, dehydrated, and mounted.

For immunofluorescence analysis, sections were treated with cold ethanol/acetone (1:1) for 1 min, blocked with 5% goat serum in MOM Mouse Ig Blocking Reagent (Vector Laboratories) at room temperature for 1 h, and then incubated with primary antibodies diluted in MOM Diluent (Vector Laboratories) overnight at 4°C. The slides were washed with PBS and incubated with Alexa Fluor 488-conjugated or Alexa Fluor 555-conjugated secondary antibodies (Molecular Probes) at room temperature for 30 min. Permount (Fisher Scientific) and TISSU MOUNT (Shiraimatsu Kikai) were used for H&E staining and immunofluorescence, respectively. Sections were observed under fluorescence microscopy (Leica DMR, Leica Microsystems).

For quantitative evaluation of muscle pathology, the percentages of myofiber with centrally located nuclei were counted for at least 1,000 fibers for each genotype ($n>4$). For evaluation of the F4/80-positive and the collagen I-positive area, the immunofluorescence signal was quantitatively measured using Image J software. Statistical analysis was performed using values represent means with standard deviations, and p values <0.05 were considered significant (Student's t-test and Mann–Whitney U test).

Results

Generation of double mutant mice exhibiting both abnormal glycosylation of α-DG and dysferlin deficiency

To generate double mutant mice, we crossed dysferlin-deficient SJL/L mice (*dysferlin*$^{sjl/sjl}$) [25] with two distinct dystroglycanopathy models, fukutin-deficient or Large-deficient mice. Previously we reported a transgenic knock-in homozygous mutant mouse carrying the retrotransposal insertion in the mouse *fukutin* ortholog (*fukutin*$^{Hp/Hp}$) [23]. Compound heterozygous mice carrying the retrotransposal insertion and a neo cassette *fukutin* disruption (*fukutin*$^{Hp/-}$) showed more abnormal glycosylation of α-DG than did mice homozygous for the insertion (*fukutin*$^{Hp/Hp}$ mice), although *fukutin*$^{Hp/-}$ mice did show a detectable amount of residual α-DG glycosylation [23]. For the current study, we generated double mutant mice with the (*dysferlin*$^{sjl/sjl}$: *fukutin*$^{Hp/-}$) genotype (Fig. 1A). The other dystroglycanopathy model, Large-deficient *Large*^{myd} mouse (*Large*$^{myd/myd}$) [27,28] show abnormal glycosylation with no detectable amount of properly glycosylated α-DG. The ligand binding activity of α-DG in *Large*$^{myd/myd}$ mice is greatly reduced compared with that in *fukutin*$^{Hp/-}$ mice [23]. Breeding strategies, genotypes, and abbreviations for these double mutant mice and their controls are shown in Figure 1A and 1B.

To confirm reduced protein expression of dysferlin and abnormal glycosylation of α-DG in these mice, we prepared solubilized fractions from skeletal muscle extracts and enriched for α-DG using wheat germ agglutinin (WGA)-agarose beads. Western blot analysis showed a dramatic reduction of dysferlin protein in skeletal muscle from (*dysferlin*$^{sjl/sjl}$: *fukutin*$^{Hp/+}$), (*dysferlin*$^{sjl/sjl}$: *fukutin*$^{Hp/-}$), (*dysferlin*$^{sjl/sjl}$: *Large*$^{myd/+}$), and (*dysferlin*$^{sjl/sjl}$: *Large*$^{myd/myd}$) mice (Fig. 1C and D). We also confirmed a significant reduction of reactivity against the monoclonal antibody IIH6, which recognizes glycosylated epitopes on α-DG that are necessary for laminin binding activity, in (*dysferlin*$^{sjl/+}$: *fukutin*$^{Hp/-}$), (*dysferlin*$^{sjl/sjl}$: *fukutin*$^{Hp/-}$), (*dysferlin*$^{sjl/+}$: *Large*$^{myd/myd}$), and (*dysferlin*$^{sjl/sjl}$: *Large*$^{myd/myd}$) (Fig. 1C and D). Overall, these data confirmed the production of model mice with four biochemically distinct genotypes in each double mutant line.

More severe muscular dystrophy in (*dysferlin*$^{sjl/sjl}$: *fukutin*$^{Hp/-}$) than in (*dysferlin*$^{sjl/sjl}$: *fukutin*$^{Hp/+}$) mice

We examined the histopathology of (*dysferlin*$^{sjl/sjl}$: *fukutin*$^{Hp/-}$) mice by hematoxylin and eosin (H&E) staining. The (*dysferlin*$^{sjl/+}$: *fukutin*$^{Hp/-}$) mice showed no obvious pathological features of muscular dystrophy (Fig. 2). The (*dysferlin*$^{sjl/sjl}$: *fukutin*$^{Hp/+}$) mice showed mild dystrophic changes such as the presence of necrotic fibers and centrally located nuclei (Fig. 2). The phenotypes of (*dysferlin*$^{sjl/+}$: *fukutin*$^{Hp/-}$) and (*dysferlin*$^{sjl/sjl}$: *fukutin*$^{Hp/+}$) mice are similar to those described previously for retrotransposon knock-in *fukutin* mutant mice and dysferlin-deficient SJL/J mice, respectively [23,25]. These results also indicate that disruption of one *dysferlin* or one *fukutin* allele does not affect the phenotype of *fukutin*$^{Hp/-}$ or *dysferlin*$^{sjl/sjl}$ single mutant mice, respectively. H&E staining showed that the (*dysferlin*$^{sjl/sjl}$: *fukutin*$^{Hp/-}$) mice showed further progressed and more severe dystrophic features than did the (*dysferlin*$^{sjl/sjl}$: *fukutin*$^{Hp/+}$) mice in quadriceps (Quad), gastrocnemius (Gast), and tibialis anterior (TA) muscles (Fig. 2A and Fig. 3A). Comparison of the percentage of muscle fibers with centrally located nuclei confirmed a more severe dystrophic phenotype in the (*dysferlin*$^{sjl/sjl}$: *fukutin*$^{Hp/-}$) mice than that in the (*dysferlin*$^{sjl/sjl}$: *fukutin*$^{Hp/+}$) mice (Fig. 2B).

To compare the pathological severity in (*dysferlin*$^{sjl/sjl}$: *fukutin*$^{Hp/-}$) and (*dysferlin*$^{sjl/sjl}$: *fukutin*$^{Hp/+}$) skeletal muscle more precisely, we counted the percentage of muscle fibers (TA) with centrally located nuclei at different ages (Fig. 3A and B). In 8-week-old mice, we observed a few fibers with centrally located nuclei and necrotic fibers in both the (*dysferlin*$^{sjl/sjl}$: *fukutin*$^{Hp/+}$) and the (*dysferlin*$^{sjl/sjl}$: *fukutin*$^{Hp/-}$) mice, but no significant differences were seen between the two (data not shown). At 15 weeks and 30 weeks of age, the (*dysferlin*$^{sjl/sjl}$: *fukutin*$^{Hp/-}$) mice show significantly more fibers with centrally located nuclei than do the (*dysferlin*$^{sjl/sjl}$: *fukutin*$^{Hp/+}$) mice (Fig. 3B). The proportion of fibers with centrally located nuclei in the (*dysferlin*$^{sjl/sjl}$: *fukutin*$^{Hp/-}$) mice increased with age. These results indicate more frequent cycles of muscle cell degeneration and regeneration in the (*dysferlin*$^{sjl/sjl}$: *fukutin*$^{Hp/-}$) mice. We next compared infiltration of macrophage and connective tissue as indicators of disease severity. Immunofluorescence analysis using the monoclonal F4/80 antibody, a marker for macrophages, indicated that macrophage infiltration was increased in (*dysferlin*$^{sjl/sjl}$: *fukutin*$^{Hp/-}$) skeletal muscle compared with (*dysferlin*$^{sjl/sjl}$: *fukutin*$^{Hp/+}$) skeletal

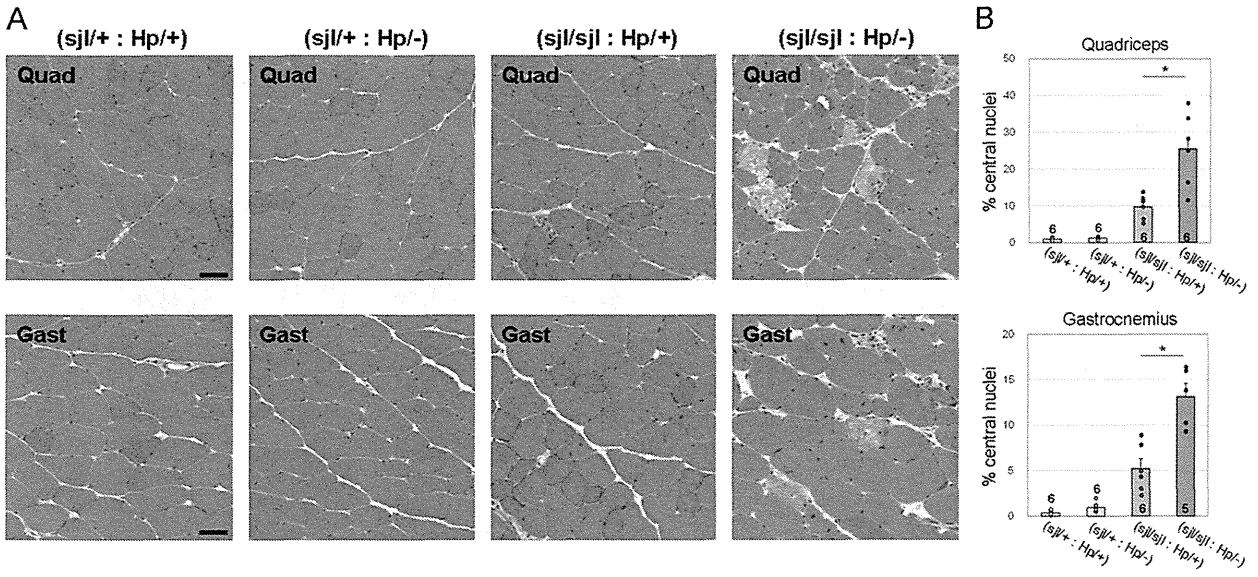

Figure 2. Histological analysis of skeletal muscle from dysferlin/fukutin double mutant mice. (A) Quadriceps (Quad) and gastrocnemius (Gast) muscle tissues from the four mouse genotypes at 15 weeks were analyzed by H&E staining. Bar, 50 μm. (B) Myofibers with centrally located nuclei were counted and quantitatively compared between (*dysferlin*$^{sjl/sjl}$: *fukutin*$^{Hp/+}$) and (*dysferlin*$^{sjl/sjl}$: *fukutin*$^{Hp/-}$) mice (*, $p<0.05$). Data shown are mean ± s.e.m. for each group (*n* is indicated in the graph). The (*dysferlin*$^{sjl/+}$: *fukutin*$^{Hp/+}$), (*dysferlin*$^{sjl/+}$: *fukutin*$^{Hp/-}$), (*dysferlin*$^{sjl/sjl}$: *fukutin*$^{Hp/+}$), and (*dysferlin*$^{sjl/sjl}$: *fukutin*$^{Hp/-}$) mice are abbreviated as (sjl/+: Hp/+), (sjl/+: Hp/−), (sjl/sjl: Hp/+), and (sjl/sjl: Hp/−), respectively.
doi:10.1371/journal.pone.0106721.g002

muscle (Fig. 4A). Quantification of F4/80-immunofluorescence signals confirmed significant increases of macrophage infiltration in (*dysferlin*$^{sjl/sjl}$: *fukutin*$^{Hp/-}$) skeletal muscle (Fig. 4B). Masson trichrome staining revealed that the fibrotic area was increased in (*dysferlin*$^{sjl/sjl}$: *fukutin*$^{Hp/-}$) skeletal muscle (Fig. 4C). Quantification of immunofluorescence signals for collagen I further supported significant increases of connective tissue infiltrations in (*dysferlin*$^{sjl/sjl}$: *fukutin*$^{Hp/-}$) skeletal muscles (Fig. 4D). These data are indicative of further progressed and more severe dystrophic phenotypes in (*dysferlin*$^{sjl/sjl}$: *fukutin*$^{Hp/-}$) skeletal muscle. Importantly, although the (*dysferlin*$^{sjl/+}$: *fukutin*$^{Hp/-}$) mice do not show muscle pathology, the (*dysferlin*$^{sjl/sjl}$: *fukutin*$^{Hp/-}$) mice show a more severe phenotype than do the (*dysferlin*$^{sjl/sjl}$: *fukutin*$^{Hp/+}$) mice, suggesting that dysferlin plays a protective role in preventing disease manifestation in the (*dysferlin*$^{sjl/+}$: *fukutin*$^{Hp/-}$) mice.

Our previous data and those of others suggest that muscle cell membrane fragility due to loss of DG or its functional glycosylation triggers disease manifestation [24,29]. However, we have not observed evidence indicating membrane fragility in *fukutin*$^{Hp/-}$ skeletal muscle [23]. To investigate whether membrane fragility is associated mechanistically with the deteriorated phenotype of the (*dysferlin*$^{sjl/sjl}$: *fukutin*$^{Hp/-}$) mice, we analyzed the population of albumin-positive muscle fibers. Intracellular albumin staining often is used as an indicator of muscle fiber damage or increased membrane permeability [30]. Immunofluorescence analysis suggested that the albumin-positive myofibers were almost absent in both (*dysferlin*$^{sjl/+}$: *fukutin*$^{Hp/+}$) and (*dysferlin*$^{sjl/+}$: *fukutin*$^{Hp/-}$) and only sparsely observed in (*dysferlin*$^{sjl/sjl}$: *fukutin*$^{Hp/+}$) skeletal muscles, whereas they appeared increased in (*dysferlin*$^{sjl/sjl}$: *fukutin*$^{Hp/-}$) skeletal muscle (Fig. 5A). Quantification of albumin-positive fibers also confirmed significant deterioration of the myofiber membrane fragility in the (*dysferlin*$^{sjl/sjl}$: *fukutin*$^{Hp/-}$) mice (Fig. 5B). These data suggest that skeletal muscle fibers in (*dysferlin*$^{sjl/+}$: *fukutin*$^{Hp/-}$) mice have latent membrane fragility, which is protected partially by dysferlin functions, and membrane fragility caused by synergy of reduced α-DG glycosylation and dysferlin-deficiency underlies the deteriorated phenotype of the (*dysferlin*$^{sjl/sjl}$: *fukutin*$^{Hp/-}$) mice.

We examined whether dysferlin itself and/or its interacting proteins, caveolin-3 [31] and MG53 [22], are compensatory upregulated in *fukutin*$^{Hp/-}$ mice. Western blot analysis showed that levels of dysferlin, caveolin-3, and MG53 were not significantly different between *fukutin*$^{Hp/-}$ and *fukutin*$^{Hp/+}$ skeletal muscle (Fig. S1A and B). Immunofluorescence analysis also showed no obvious change in dysferlin expression pattern between *fukutin*$^{Hp/-}$ and *fukutin*$^{Hp/+}$ skeletal muscle (Fig. S1C).

Characterization of muscular dystrophic changes in (*dysferlin*$^{sjl/sjl}$: *Large*$^{myd/myd}$) mice

We subsequently analyzed the histopathology of (*dysferlin*$^{sjl/sjl}$: *Large*$^{myd/myd}$) mice. *Large*$^{myd/myd}$ mice show severe muscular dystrophic phenotypes such as infiltration of connective and fat tissues and marked variation in fiber size [28]. Almost all α-DG is hypoglycosylated in *Large*$^{myd/myd}$ mice [23]. We confirmed that the pathology of (*dysferlin*$^{sjl/+}$: *Large*$^{myd/myd}$) mice was more severe than that in (*dysferlin*$^{sjl/sjl}$: *Large*$^{myd/+}$) mice (Fig. 6). To examine whether the dysferlin functions have protective roles in *Large*$^{myd/myd}$ skeletal muscle, we compared the pathology in (*dysferlin*$^{sjl/+}$: *Large*$^{myd/myd}$) and (*dysferlin*$^{sjl/sjl}$: *Large*$^{myd/myd}$) mice. The (*dysferlin*$^{sjl/+}$: *Large*$^{myd/myd}$) mice showed necrotic and centrally nucleated fibers, indicating frequent cycles of muscle degeneration and regeneration (Fig. 6C). In addition, some animals showed signs of advanced muscular dystrophic changes such as variations in fiber size and connective tissue infiltration (Fig. 6D). The (*dysferlin*$^{sjl/sjl}$: *Large*$^{myd/myd}$) mice exhibited severe pathology, including marked variation in fiber size and large areas with infiltration (Fig. 6E and F). We evaluated these pathologies quantitatively by measuring the areas of macrophage or connective tissue infiltration and the population of albumin-positive

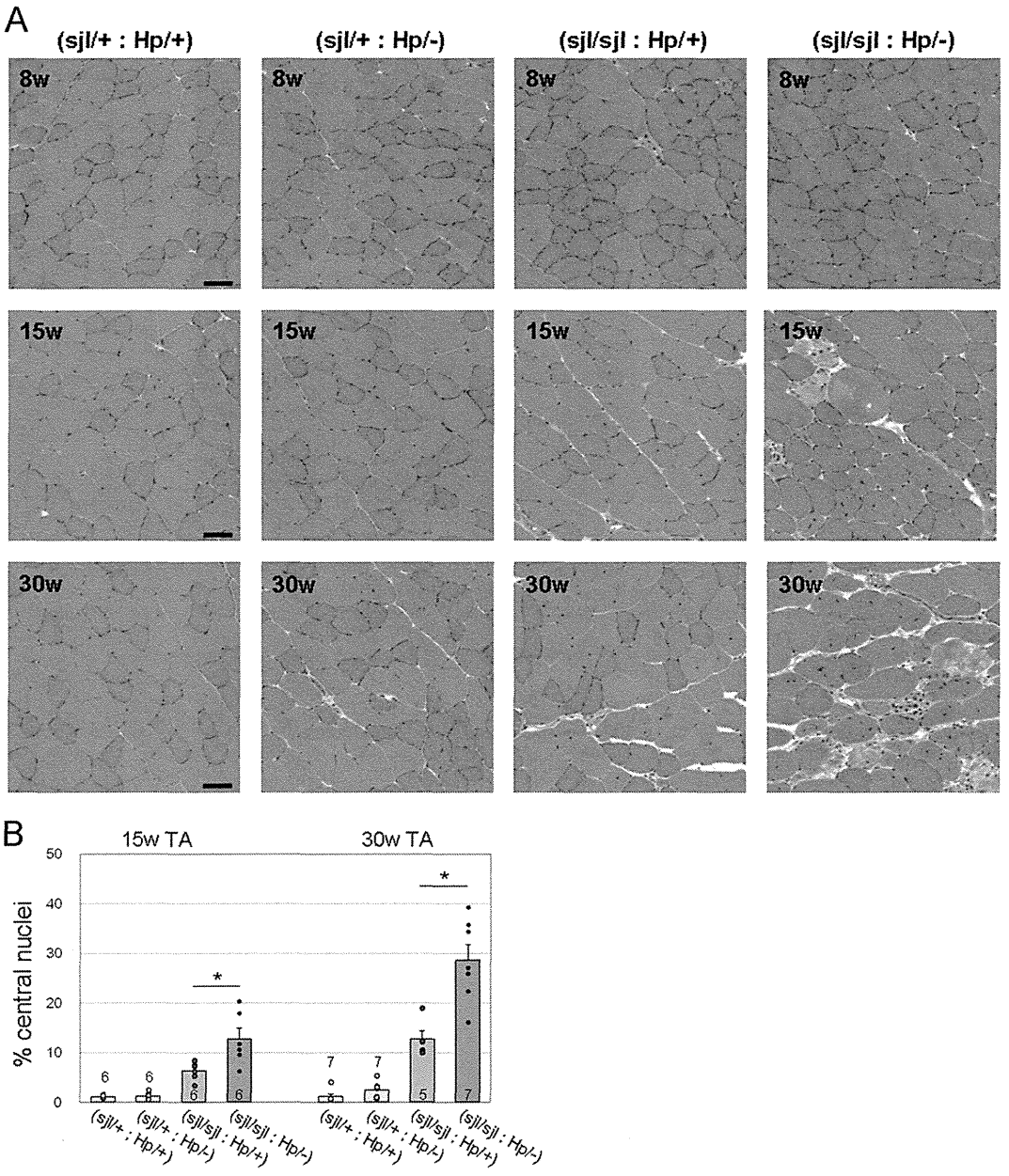

Figure 3. Pathological comparisons between (*dysferlin*$^{sjl/sjl}$: *fukutin*$^{Hp/+}$) and (*dysferlin*$^{sjl/sjl}$ and *fukutin*$^{Hp/-}$) mice. (A) H&E staining of TA muscle from (*dysferlin*$^{sjl/+}$: *fukutin*$^{Hp/+}$), (*dysferlin*$^{sjl/+}$: *fukutin*$^{Hp/-}$), (*dysferlin*$^{sjl/sjl}$: *fukutin*$^{Hp/+}$) and (*dysferlin*$^{sjl/sjl}$: *fukutin*$^{Hp/-}$) mice at 8, 15 and 30 weeks. Bar, 50 μm. (B) Myofibers with centrally located nuclei were counted and quantitatively compared between (*dysferlin*$^{sjl/sjl}$: *fukutin*$^{Hp/+}$) and (*dysferlin*$^{sjl/sjl}$: *fukutin*$^{Hp/-}$) mice at 15 and 30 weeks (*, $p < 0.05$). Data shown are mean ± s.e.m. for each group (*n* is indicated in the graph). The (*dysferlin*$^{sjl/+}$: *fukutin*$^{Hp/+}$), (*dysferlin*$^{sjl/+}$: *fukutin*$^{Hp/-}$), (*dysferlin*$^{sjl/sjl}$: *fukutin*$^{Hp/+}$), and (*dysferlin*$^{sjl/sjl}$: *fukutin*$^{Hp/-}$) mice are abbreviated as (sjl/+: Hp/+), (sjl/+: Hp/−), (sjl/sjl: Hp/+), and (sjl/sjl: Hp/−), respectively.
doi:10.1371/journal.pone.0106721.g003

muscle fibers (Fig. 6I, J, and K). Both the macrophage-infiltrated area and the population of albumin-positive muscle fibers tended to be larger in (*dysferlin*$^{sjl/sjl}$: *Large*$^{myd/myd}$) than in (*dysferlin*$^{sjl/+}$: *Large*$^{myd/myd}$); however, we did not observe statistically significant differences between the two groups. Furthermore, quantification of collagen I immunofluorescence showed no significant difference in connective tissue infiltration between (*dysferlin*$^{sjl/sjl}$: *Large*$^{myd/myd}$) and (*dysferlin*$^{sjl/+}$: *Large*$^{myd/myd}$) skeletal muscles. These results suggest that dysferlin function produces limited protective effects against the progression of severe muscular dystrophy in *Large*$^{myd/myd}$ mice. Interestingly, however, when compared with the (*dysferlin*$^{+/+}$: *Large*$^{myd/myd}$) mice, the (*dysferlin*$^{sjl/sjl}$: *Large*$^{myd/myd}$) mice showed significant increases in F4/80, collagen I and intracellular albumin staining (Fig. 6I, J, and K). The amount of dysferlin protein in total lysates from (*dysferlin*$^{sjl/sjl}$: *Large*$^{myd/myd}$) and (*dysferlin*$^{sjl/+}$: *Large*$^{myd/myd}$) skeletal muscles was estimated to

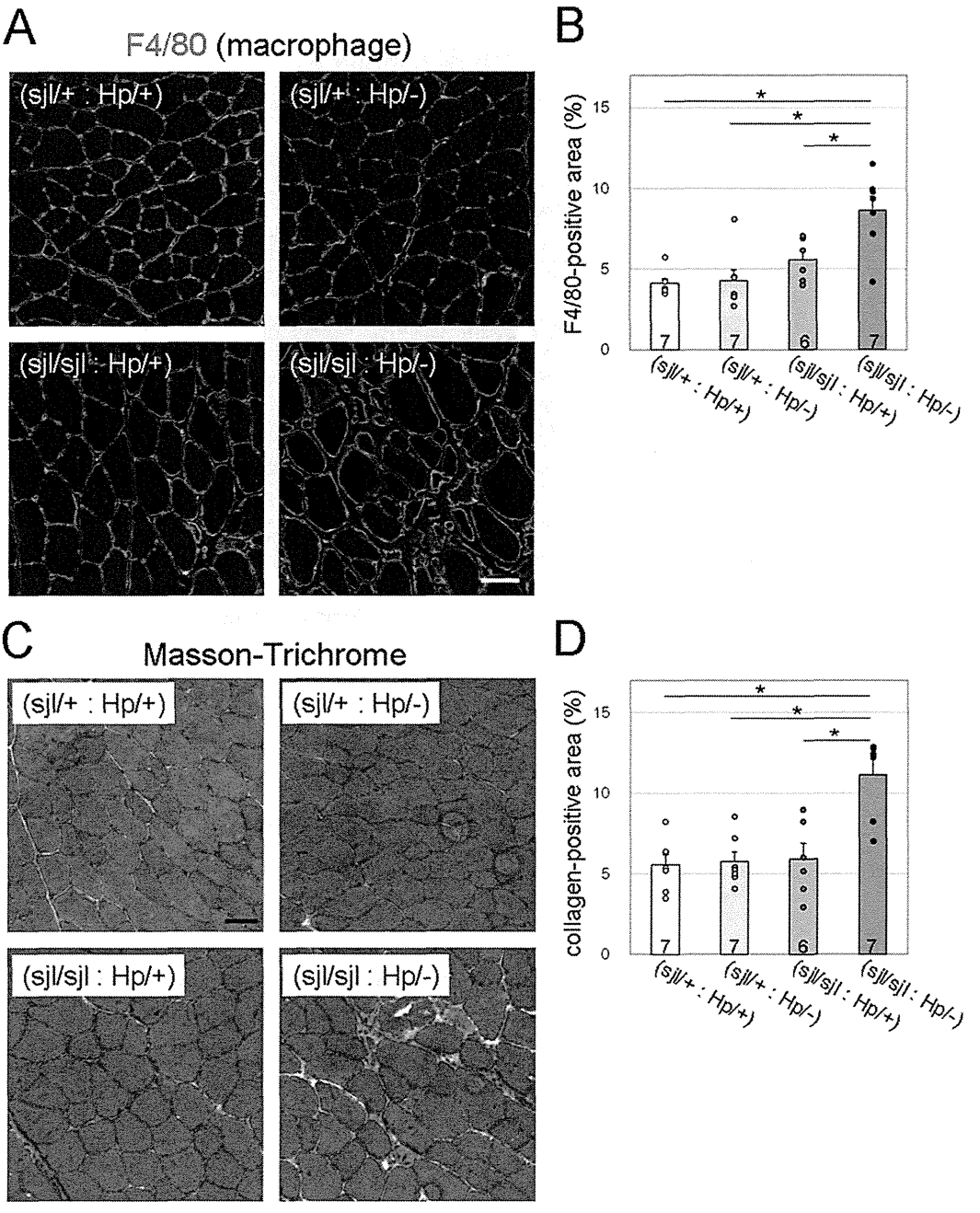

Figure 4. Macrophage and connective tissue infiltration in dysferlin/fukutin double mutant mice. (A) Macrophage infiltration was determined by immunofluorescence analysis using the F4/80 antibody (red). The sarcolemma and nuclei were stained by laminin (green) and DAPI (blue), respectively. TA muscle sections from 30-week-old mice were used. Bar, 50 μm. (B) F4/80-positive immunofluorescence signals were quantified using Image J software. (C) Connective tissue infiltration was determined by Masson-Trichrome staining. TA muscle sections from 30-week-old mice were used. Bar, 50 μm. (D) Quantitative analysis of connective tissue infiltration, determined by immunofluorescence analysis using anti-collagen I antibody. The collagen I-positive area was quantified using Image J software. For quantitative analysis (B and D), data shown are mean ± s.e.m. for each group (*n* is indicated in the graph; *, $p<0.05$). The (*dysferlin*$^{sjl/+}$: *fukutin*$^{Hp/+}$), (*dysferlin*$^{sjl/+}$: *fukutin*$^{Hp/-}$), (*dysferlin*$^{sjl/sjl}$: *fukutin*$^{Hp/+}$), and (*dysferlin*$^{sjl/sjl}$: *fukutin*$^{Hp/-}$) mice are abbreviated as (sjl/+: Hp/+), (sjl/+: Hp/−), (sjl/jl: Hp/+), and (sjl/sjl: Hp/−), respectively.
doi:10.1371/journal.pone.0106721.g004

be ~20% and ~60% of that from (*dysferlin*$^{+/+}$: *Large*$^{myd/myd}$) muscle, respectively (Fig. 6L). These results suggest that the dramatic reduction in the amount/activity of dysferlin protein may be associated with a worse phenotype in the (*dysferlin*$^{sjl/sjl}$: *Large*$^{myd/myd}$) mice. Overall, our results suggest that the protective effects of dysferlin on dystroglycanopathy phenotype appear to be diminished when the dystrophic pathology is severe and progressive and also may depend on the amount of dysferlin proteins.

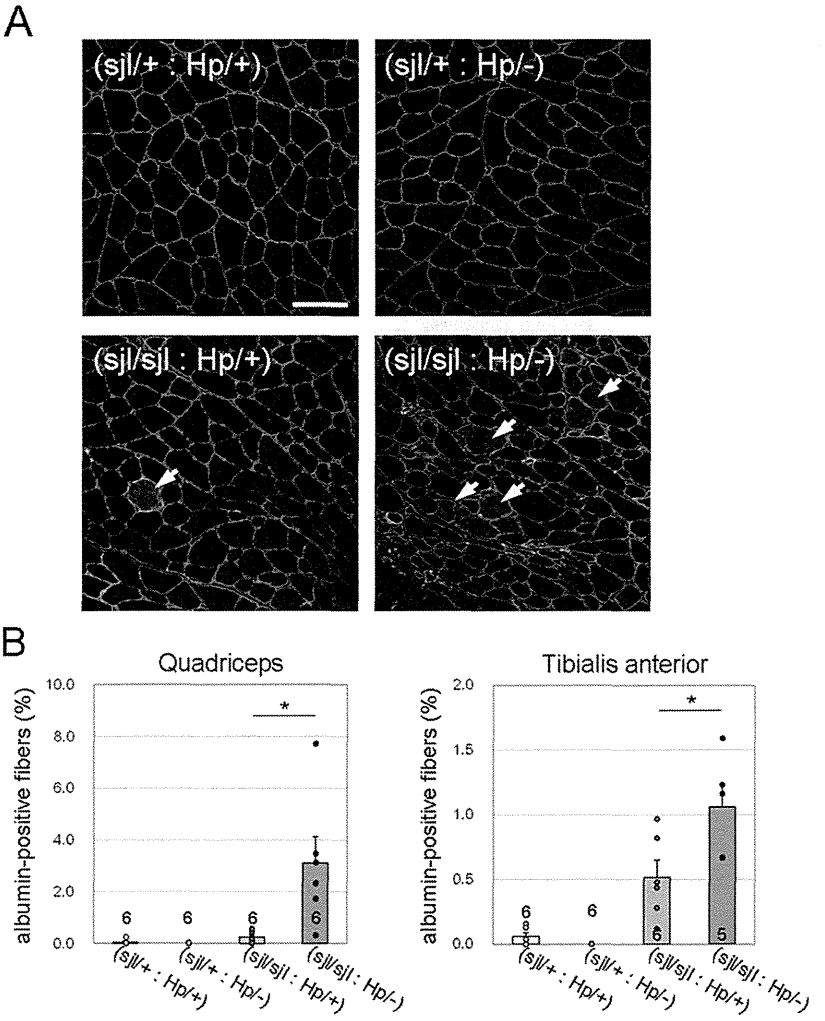

Figure 5. Myofiber membrane fragility in dysferlin/fukutin double mutant mice. (A) Intracellular albumin was determined by immunofluorescence (red). Myofibers are marked by laminin staining (green). Arrows indicate myofibers with intracellular albumin. Images were taken from quadriceps muscle sections of 15-week-old mice. Bar, 100 μm. (B) Myofibers with intracellular albumin were counted and statistically compared between (*dysferlin*$^{sjl/sjl}$: *fukutin*$^{Hp/+}$) and (*dysferlin*$^{sjl/sjl}$: *fukutin*$^{Hp/-}$) mice. Quadriceps and TA muscle sections from 15-week-old mice were analyzed. Data shown are mean ± s.e.m. for each group (*n* is indicated in the graph; *, $p<0.05$). The (*dysferlin*$^{sjl/+}$: *fukutin*$^{Hp/+}$), (*dysferlin*$^{sjl/+}$: *fukutin*$^{Hp/-}$), (*dysferlin*$^{sjl/sjl}$: *fukutin*$^{Hp/+}$), and (*dysferlin*$^{sjl/sjl}$: *fukutin*$^{Hp/-}$) mice are abbreviated as (sjl/+: Hp/+), (sjl/+: Hp/−), (sjl/sjl: Hp/+), and (sjl/sjl: Hp/−), respectively.
doi:10.1371/journal.pone.0106721.g005

Discussion

Here we have characterized the contribution of dysferlin-deficiency to the pathology of dystroglycanopathy using double mutant mice for dysferlin and α-DG glycosylation. To date, several dystroglycanopathy model mice have been established. *Large*^{myd} mice [28] and knock-in mice carrying the FKRP P448L mutation [32] show no detectable amounts of functionally glycosylated α-DG, no laminin binding activity, and progressive muscular dystrophy. On the other hand, other dystroglycanopathy mouse models do not show a muscular dystrophy phenotype [23]. We previously reported that a small amount of intact α-DG in *fukutin*$^{Hp/-}$ mice is sufficient to maintain muscle cell integrity, thus preventing muscular dystrophy [23]. These results and others suggest that the presence of functionally glycosylated α-DG can decrease disease severity [33,34]. In the present study, however, we showed that although (*dysferlin*$^{sjl/+}$: *fukutin*$^{Hp/-}$) mice did not exhibit a muscular dystrophy phenotype, (*dysferlin*$^{sjl/sjl}$: *fukutin*$^{Hp/-}$) mice developed a more exacerbated phenotype than did the *dysferlin* single-mutant (*dysferlin*$^{sjl/sjl}$: *fukutin*$^{Hp/+}$) mice. It has been widely accepted that α-DG glycosylation plays an important role in preventing disease-causing membrane fragility by maintaining a tight association between the basement membrane and the muscle cell membrane, and its defects produce muscle membrane that is susceptible to damage [24,29]. The synergically exacerbated phenotype of the (*dysferlin*$^{sjl/sjl}$: *fukutin*$^{Hp/-}$) mice suggests latent membrane fragility in *fukutin*-deficient *fukutin*$^{Hp/-}$ skeletal muscle. Indeed, the increased number of intracellular albumin-positive fibers in the (*dysferlin*$^{sjl/sjl}$: *fukutin*$^{Hp/-}$) mice also supports this hypothesis. It is assumed in the *fukutin*$^{Hp/-}$ myofiber that interaction between the basement membrane and the cell membrane may be weakened, and therefore disease-causative membrane damage could occur during

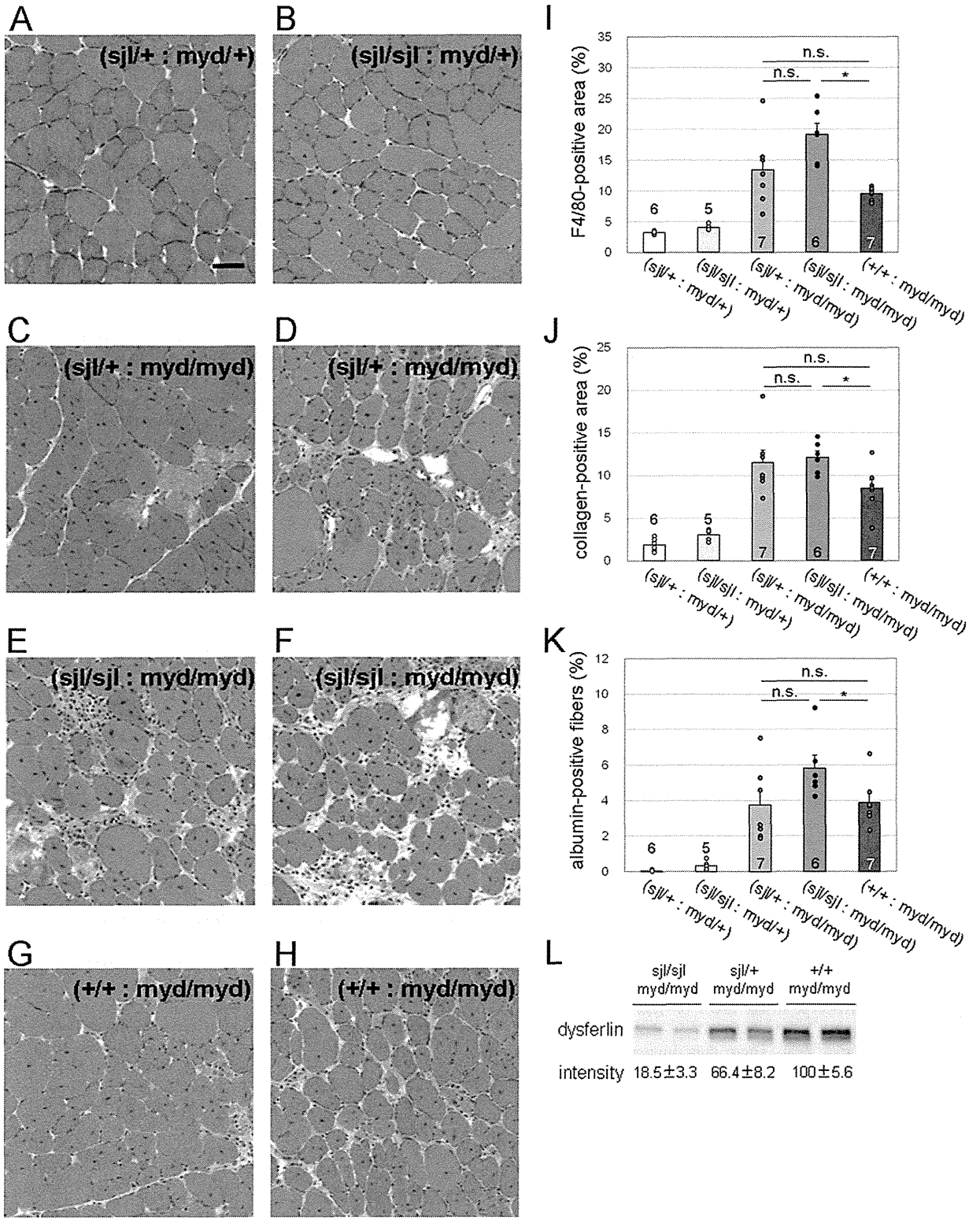

Figure 6. Histopathological analysis of skeletal muscle from dysferlin/Large double mutant mice. (A–H) H&E staining of TA muscle from [(*dysferlin*$^{sjl/+}$: *Large*$^{myd/+}$), A], [(*dysferlin*$^{sjl/sjl}$: *Large*$^{myd/+}$), B], [(*dysferlin*$^{sjl/+}$: *Large*$^{myd/myd}$), C and D], [(*dysferlin*$^{sjl/sjl}$: *Large*$^{myd/myd}$), E and F], and [(*dysferlin*$^{+/+}$: *Large*$^{myd/myd}$), G and H] mice at 15 weeks. Bar, 50 μm. (I) Quantitative analysis of macrophage infiltration, determined by immunofluorescence analysis using F4/80 antibody. (J) Quantitative analysis of connective tissue infiltration determined by immunofluorescence analysis using

anti-collagen I antibody. (K) Quantitative analysis of the proportion of myofibers containing intracellular albumin. For quantitative analysis (I–K), data shown are mean ± s.e.m. for each group (*n* is indicated in the graph; *, $p<0.05$; n.s., not significant). (L) Western blot analysis and quantification of dysferlin expression in the total skeletal muscle lysate from (*dysferlin*$^{sjl/sjl}$: *Large*$^{myd/myd}$), (*dysferlin*$^{sjl/+}$: *Large*$^{myd/myd}$), and (*dysferlin*$^{+/+}$: *Large*$^{myd/myd}$) mice. A representative two individual samples are shown in the blot. Data shown are the average of three individual mice with standard deviations. The (*dysferlin*$^{sjl/+}$: *Large*$^{myd/+}$), (*dysferlin*$^{sjl/sjl}$: *Large*$^{myd/+}$), (*dysferlin*$^{sjl/+}$: *Large*$^{myd/myd}$), (*dysferlin*$^{sjl/sjl}$: *Large*$^{myd/myd}$), and (*dysferlin*$^{+/+}$: *Large*$^{myd/myd}$) mice are abbreviated as (sjl/+: myd/+), (sjl/sjl: myd/+), (sjl/+: myd/myd), (sjl/sjl: myd/myd), and (+/+: myd/myd), respectively.
doi:10.1371/journal.pone.0106721.g006

muscle contractions. However, such presumable membrane fragility may be protected in part by the dysferlin functions.

It is known that dysferlin plays a role in membrane repair pathway and several proteins are known to interact with dysferlin, suggesting that dysferlin forms a protein complex during the membrane repair process. MG53 has been shown to interact with dysferlin and participate in membrane repair, and genetic disruption of MG53 in mice results in muscular dystrophy [22]. Caveolin-3 is known to interact with dysferlin and MG53 [31,35]. In the present study, however, we did not observe compensatory upregulation of these proteins in *fukutin*$^{Hp/-}$ mice, suggesting that dysferlin functions other than membrane repair may play protective roles in the *fukutin*$^{Hp/-}$ mice. Recently, accumulating evidence has suggested new dysferlin roles other than membrane repair, such as T-tubule formation, maintenance, and stabilizing stress-induced Ca^{2+} signaling [36,37]. In addition, it has been reported that dysferlin deficiency leads to increased expression of complement factors and that complement-mediated muscle injury is associated with the pathogenesis of dysferlin-deficient muscular dystrophy [38]. Therefore, it is possible that such impairments independently or synergically contribute to the pathology of the double mutant mice.

Our results showed, rather unexpectedly, that the double-mutant (*dysferlin*$^{sjl/sjl}$: *Large*$^{myd/myd}$) mice did not exhibit significant deterioration of muscle pathology compared with the single-mutant (*dysferlin*$^{sjl/+}$: *Large*$^{myd/myd}$) mice. These data suggest that the protective effects of dysferlin in *Large*$^{myd/myd}$ mice were slightly or much reduced compared with those in *fukutin*$^{Hp/-}$ mice. Since *Large*$^{myd/myd}$ mice showed severe and rapid progressive pathology while *fukutin*$^{Hp/-}$ mice were asymptomatic, our data suggest that the protective effect of dysferlin may be less when disease pathology is advanced and/or severe. It has been reported that a double mutant of dysferlin and dystrophin produced a more exacerbated phenotype than did either single mutant [39]. In our colony, *Large*$^{myd/myd}$ mice show much more severe and rapid progressive pathology than do dystrophin-deficient mdx mice, supporting our hypothesis of a limited protective effect of dysferlin in dystrophic pathology. Interestingly, the (*dysferlin*$^{sjl/sjl}$: *Large*$^{myd/myd}$) mice, however, showed a significantly worse phenotype that did the (*dysferlin*$^{+/+}$: *Large*$^{myd/myd}$) mice. In addition, there is a tendency toward a worse phenotype in the order of dysferlin amount, *i.e.* (*dysferlin*$^{+/+}$: *Large*$^{myd/myd}$), (*dysferlin*$^{sjl/+}$: *Large*$^{myd/myd}$), and (*dysferlin*$^{sjl/sjl}$: *Large*$^{myd/myd}$). These data support the possibility that the protective effect of dysferlin is present even in the severe dystrophic *Large*$^{myd/myd}$ mice. We conclude that dysferlin has the potential to protect muscular dystrophy progression; however, its effect may depend on disease severity and the amount/activity of dysferlin proteins.

Recently, we showed that the retrotransposal insertion in the 3′-UTR region of *fukutin* causes abnormal mRNA splicing, which is induced by a strong splice acceptor site in SVA and a rare alternative donor site in the last exon, to produce an aberrantly spliced fukutin protein [7]. The introduction of antisense oligonucleotides that target the splice acceptor, the predicted exonic splicing enhancer, and the intronic splicing enhancer prevented the pathogenic exon trapping by SVA in the cells of FCMD patients as well as model mice (*fukutin*$^{Hp/Hp}$ and *fukutin*$^{Hp/-}$) [7]. This therapeutic strategy can potentially be applied to almost all FCMD patients in Japan, and can therefore be the first radical clinical treatment for dystroglycanopathies. However, there was no animal model to test the effectiveness of the antisense oligonucleotide therapy. Since *fukutin*$^{Hp/-}$ mice do not exhibit any signs of muscular dystrophy [23], they are not a great model for examining therapeutic effects of this strategy. Skeletal muscle-selective fukutin cKO mice, MCK-fukutin-cKO and Myf5-fukutin-cKO, showed dystrophic pathology [24], but they do not possess the retrotransposal insertion, and thus they are not applicable for testing the antisense oligonucleotide therapy. Our present study demonstrates more severe dystrophic phenotype of (*dysferlin*$^{sjl/sjl}$: *fukutin*$^{Hp/-}$) mice compared with (*dysferlin*$^{sjl/sjl}$: *fukutin*$^{Hp/+}$) mice. Since the (*dysferlin*$^{sjl/sjl}$: *fukutin*$^{Hp/-}$) mice possess the retrotransposal insertion and show dystrophic phenotype, they will be used as the first model for evaluation of the antisense oligonucleotide therapy for FCMD. There is a possibility that the absence of dysferlin could add hurdles on how to interpret the results of the antisense oligonucleotide treatments; however, our quantitative assessments established in this study could overcome this issue. For example, macrophage infiltration (Fig. 4B), connective tissue infiltration (Fig. 4D), and membrane fragility in quadriceps muscles (Fig. 5B) were significantly increased only in the (*dysferlin*$^{sjl/sjl}$: *fukutin*$^{Hp/-}$) mice. These parameters in the (*dysferlin*$^{sjl/sjl}$: *fukutin*$^{Hp/+}$) mice were not changed compared with those in the (*dysferlin*$^{sjl/+}$: *fukutin*$^{Hp/+}$) and the (*dysferlin*$^{sjl/+}$: *fukutin*$^{Hp/-}$) mice, and therefore can be used for quantitative evaluation for therapeutic effects of the antisense oligonucleotide treatments. We hope that generation of this novel FCMD model and establishment of the quantitative evaluation for disease severity will accelerate the future translational researches to overcome FCMD.

Supporting Information

Figure S1 Expression of dysferlin and dysferlin-interacting proteins in *fukutin*$^{Hp/-}$ mice. (A) Western blot analysis of dysferlin, caveolin-3, and MG53 in skeletal muscle extracts from fukutin-deficient *fukutin*$^{Hp/-}$ (Hp/−), and control *fukutin*$^{Hp/+}$ (Hp/+) mice. A representative two individual samples for each mouse line are shown in the blots. (B) Quantification of protein expression (panel A) was shown in graphs. Data shown are the average with standard deviations ($n = 4$ for dysferlin, $n = 3$ for caveolin-3 and MG53). (C) Immunofluorescence analysis of dysferlin in *fukutin*$^{Hp/-}$ (Hp/−) and *fukutin*$^{Hp/+}$ (Hp/+) mice. Bar, 50 μm.
(DOCX)

Acknowledgments

We would like to thank past and present members of the Dr. Toda's laboratory for fruitful discussions and scientific contributions. We also thank Dr. Jennifer Logan for help in editing the manuscript.

Author Contributions

Conceived and designed the experiments: MK ZL TT. Performed the experiments: MK ZL CI KM. Analyzed the data: MK CI. Contributed reagents/materials/analysis tools: CM KM. Contributed to the writing of the manuscript: MK TT.

References

1. Davies KE, Nowak KJ (2006) Molecular mechanisms of muscular dystrophies: old and new players. Nat Rev Mol Cell Biol 7: 762–773.
2. Barresi R, Campbell KP (2006) Dystroglycan: from biosynthesis to pathogenesis of human disease. J Cell Sci 119: 199–207.
3. Michele DE, Barresi R, Kanagawa M, Saito F, Cohn RD, et al. (2002) Post-translational disruption of dystroglycan-ligand interactions in congenital muscular dystrophies. Nature 418: 417–422.
4. Yoshida-Moriguchi T, Yu L, Stalnaker SH, Davis S, Kunz S, et al. (2010) O-mannosyl phosphorylation of alpha-dystroglycan is required for laminin binding. Science 327: 88–92.
5. Fukuyama Y, Osawa M, Suzuki H (1981) Congenital progressive muscular dystrophy of the Fukuyama type - clinical, genetic and pathological considerations. Brain Dev 3: 1–29.
6. Kobayashi K, Nakahori Y, Miyake M, Matsumura K, Kondo-Iida E, et al. (1998) An ancient retrotransposal insertion causes Fukuyama-type congenital muscular dystrophy. Nature 394: 388–392.
7. Taniguchi-Ikeda M, Kobayashi K, Kanagawa M, Yu CC, Mori K, et al. (2011) Pathogenic exon-trapping by SVA retrotransposon and rescue in Fukuyama muscular dystrophy. Nature 478: 127–131.
8. Godfrey C, Clement E, Mein R, Brockington M, Smith J, et al. (2007) Refining genotype phenotype correlations in muscular dystrophies with defective glycosylation of dystroglycan. Brain 130: 2725–2735.
9. Wells L (2013) The O-Mannosylation Pathway: Glycosyltransferases and Proteins Implicated in Congenital Muscular Dystrophy. J Biol Chem 288: 6930–6935.
10. Vuillaumier-Barrot S, Bouchet-Séraphin C, Chelbi M, Devisme L, Quentin S, et al. (2012) Identification of mutations in TMEM5 and ISPD as a cause of severe cobblestone lissencephaly. Am J Hum Genet 91: 1135–1143.
11. Jae LT, Raaben M, Riemersma M, van Beusekom E, Blomen VA, et al. (2013) Deciphering the glycosylome of dystroglycanopathies using haploid screens for lassa virus entry. Science 340: 479–483.
12. Buysse K, Riemersma M, Powell G, van Reeuwijk J, Chitayat D, et al. (2013) Missense mutations in β-1,3-N-acetylglucosaminyltransferase 1 (B3GNT1) cause Walker-Warburg syndrome. Hum Mol Genet 22: 1746–1754.
13. Stevens E, Carss KJ, Cirak S, Foley AR, Torelli S, et al. (2013) Mutations in B3GALNT2 cause congenital muscular dystrophy and hypoglycosylation of α-dystroglycan. Am J Hum Genet 92: 354–365.
14. Carss KJ, Stevens E, Foley AR, Cirak S, Riemersma M, et al. (2013) Mutations in GDP-mannose pyrophosphorylase B cause congenital and limb-girdle muscular dystrophies associated with hypoglycosylation of α-dystroglycan. Am J Hum Genet 93: 29–41.
15. Yoshida A, Kobayashi K, Manya H, Taniguchi K, Kano H, et al. (2001) Muscular dystrophy and neuronal migration disorder caused by mutations in a glycosyltransferase, POMGnT1. Dev Cell 1: 717–724.
16. Manya H, Chiba A, Yoshida A, Wang X, Chiba Y, et al. (2004) Demonstration of mammalian protein O-mannosyltransferase activity: coexpression of POMT1 and POMT2 required for enzymatic activity. Proc Natl Acad Sci USA 101: 500–505.
17. Inamori K, Yoshida-Moriguchi T, Hara Y, Anderson ME, Yu L, et al. (2012) Dystroglycan function requires xylosyl- and glucuronyltransferase activities of LARGE. Science 335: 93–96.
18. Yoshida-Moriguchi T, Willer T, Anderson ME, Venzke D, Whyte T, et al. (2013) SGK196 Is a Glycosylation-Specific O-Mannose Kinase Required for Dystroglycan Function. Science 341: 896–899.
19. Kuga A, Kanagawa M, Sudo A, Chan YM, Tajiri M, et al. (2012) Absence of post-phosphoryl modification in dystroglycanopathy mouse models and wild-type tissues expressing non-laminin binding form of α-dystroglycan. J Biol Chem 287: 9560–9567.
20. Mariano A, Henning A, Han R (2013) Dysferlin-deficient muscular dystrophy and innate immune activation. FEBS J 280: 4165–4176.
21. Bansal D, Miyake K, Vogel SS, Groh S, Chen CC, et al. (2003) Defective membrane repair in dysferlin-deficient muscular dystrophy. Nature 423: 168–172.
22. Cai C, Masumiya H, Weisleder N, Matsuda N, Nishi M, et al. (2009) MG53 nucleates assembly of cell membrane repair machinery. Nat Cell Biol 11: 56–64.
23. Kanagawa M, Nishimoto A, Chiyonobu T, Takeda S, Miyagoe-Suzuki Y, et al. (2009) Residual laminin-binding activity and enhanced dystroglycan glycosylation by LARGE in novel model mice to dystroglycanopathy. Hum Mol Genet 18: 621–631.
24. Kanagawa M, Yu CC, Ito C, Fukada S, Hozoji-Inada M, et al. (2013) Impaired viability of muscle precursor cells in muscular dystrophy with glycosylation defects and amelioration of its severe phenotype by limited gene expression. Hum Mol Genet 22: 3003–3015.
25. Bittner RE, Anderson LV, Burkhardt E, Bashir R, Vafiadaki E, et al. (1999) Dysferlin deletion in SJL mice (SJL-Dysf) defines a natural model for limb girdle muscular dystrophy 2B. Nat Genet 23: 141–142.
26. Kurahashi H, Taniguchi M, Meno C, Taniguchi Y, Takeda S, et al. (2005) Basement membrane fragility underlies embryonic lethality in fukutin-null mice. Neurobiol Dis 19: 208–217.
27. Grewal PK, Holzfeind PJ, Bittner RE, Hewitt JE (2001) Mutant glycosyltransferase and altered glycosylation of alpha-dystroglycan in the myodystrophy mouse. Nat Genet 28: 151–154.
28. Holzfeind PJ, Grewal PK, Reitsamer HA, Kechvar J, Lassmann H, et al. (2002) Skeletal, cardiac and tongue muscle pathology, defective retinal transmission, and neuronal migration defects in the Large(myd) mouse defines a natural model for glycosylation-deficient muscle-eye-brain disorders. Hum Mol Genet 11: 2673–2687.
29. Han R, Kanagawa M, Yoshida-Moriguchi T, Rader EP, Ng RA, et al. (2009) Basal lamina strengthens cell membrane integrity via the laminin G domain-binding motif of alpha-dystroglycan. Proc Natl Acad Sci USA 106: 12573–12579.
30. Straub V, Rafael JA, Chamberlain JS, Campbell KP (1997) Animal models for muscular dystrophy show different patterns of sarcolemmal disruption. J Cell Biol 139: 375–385.
31. Matsuda C, Hayashi YK, Ogawa M, Aoki M, Murayama K, et al. (2001) The sarcolemmal proteins dysferlin and caveolin-3 interact in skeletal muscle. Hum Mol Genet 10: 1761–1766.
32. Chan YM, Keramaris-Vrantsis E, Lidov HG, Norton JH, Zinchenko N, et al. (2010) Fukutin-related protein is essential for mouse muscle, brain and eye development and mutation recapitulates the wide clinical spectrums of dystroglycanopathies. Hum Mol Genet 19: 3995–4006.
33. Wang CH, Chan YM, Tang RH, Xiao B, Lu P, et al. (2011) Post-natal knockdown of fukutin-related protein expression in muscle by long-term RNA interference induces dystrophic pathology. Am J Pathol 178: 261–272.
34. Murakami T, Hayashi YK, Noguchi S, Ogawa M, Nonaka I, et al. (2006) Fukutin gene mutations cause dilated cardiomyopathy with minimal muscle weakness. Ann Neurol 60: 597–602.
35. Cai C, Weisleder N, Ko JK, Komazaki S, Sunada Y, et al. (2009) Membrane repair defects in muscular dystrophy are linked to altered interaction between MG53, caveolin-3, and dysferlin. J Biol Chem 284: 15894–15902.
36. Klinge L, Harris J, Sewry C, Charlton R, Anderson L, et al. (2010) Dysferlin associates with the developing T-tubule system in rodent and human skeletal muscle. Muscle Nerve 41: 166–173.
37. Kerr JP, Ziman AP, Mueller AL, Muriel JM, Kleinhans-Welte E, et al. (2013) Dysferlin stabilizes stress-induced Ca^{2+} signaling in the transverse tubule membrane. Proc Natl Acad Sci USA 110: 20831–20836.
38. Han R, Frett EM, Levy JR, Rader EP, Lueck JD, et al. (2010) Genetic ablation of complement C3 attenuates muscle pathology in dysferlin-deficient mice. J Clin Invest 120: 4366–4374.
39. Han R, Rader EP, Levy JR, Bansal D, Campbell KP (2011) Dystrophin deficiency exacerbates skeletal muscle pathology in dysferlin-null mice. Skelet Muscle 1: 35.

ANNALS of Clinical and Translational Neurology
Open Access
ANA American Neurological Association

BRIEF COMMUNICATION

ABCG2 variant has opposing effects on onset ages of Parkinson's disease and gout

Hirotaka Matsuo[1], Hiroyuki Tomiyama[2], Wataru Satake[3], Toshinori Chiba[1], Hiroyuki Onoue[4], Yusuke Kawamura[1], Akiyoshi Nakayama[1], Seiko Shimizu[1], Masayuki Sakiyama[1], Manabu Funayama[2], Kenya Nishioka[2], Toru Shimizu[5], Kenichi Kaida[4], Keiko Kamakura[4,6], Tatsushi Toda[3], Nobutaka Hattori[2] & Nariyoshi Shinomiya[1]

[1]Department of Integrative Physiology and Bio-Nano Medicine, National Defense Medical College, Tokorozawa, Japan
[2]Department of Neurology, Juntendo University School of Medicine, Tokyo, Japan
[3]Division of Neurology/Molecular Brain Science, Kobe University Graduate School of Medicine, Kobe, Japan
[4]Department of Internal Medicine, National Defense Medical College, Tokorozawa, Japan
[5]Midorigaoka Hospital, Osaka, Japan
[6]Department of Physical Therapy, School of Health Sciences, Tokyo University of Technology, Tokyo, Japan

Correspondence
Hirotaka Matsuo, Department of Integrative Physiology and Bio-Nano Medicine, National Defense Medical College, 3-2 Namiki, Tokorozawa, Saitama 359-8513, Japan. Tel: +81-4-2995-1482; Fax: +81-4-2996-5187; E-mail: hmatsuo@ndmc.ac.jp

Funding Information
Supported by grants from the Ministry of Education, Culture, Sports, Science, and Technology of Japan, the Ministry of Health, Labour and Welfare of Japan, the Ministry of Defense of Japan, the Japan Society for the Promotion of Science, the Kawano Masanori Memorial Foundation for Promotion of Pediatrics, and the Gout Research Foundation of Japan.

Received: 6 November 2014; Accepted: 30 November 2014

Annals of Clinical and Translational Neurology **2015; 2(3): 302–306**

doi: 10.1002/acn3.167

Abstract

Uric acid (urate) has been suggested to play a protective role in Parkinson's disease onset through its antioxidant activity. Dysfunction of ABCG2, a high-capacity urate exporter, is a major cause for early-onset gout based on hyperuricemia. In this study, the effects of a dysfunctional *ABCG2* variant (Q141K, rs2231142) were analyzed on the ages at onset of gout patients ($N = 507$) and Parkinson's disease patients ($N = 1015$). The Q141K variant hastened the gout onset ($P = 0.0027$), but significantly associated with later Parkinson's disease onset ($P = 0.025$). Our findings will be helpful for development of more effective prevention of Parkinson's disease.

Introduction

Parkinson's disease (PD) is a multifactorial disease characterized by selective cell death of dopaminergic neurons. Oxidative stress is well known to be one of the major causes of PD development.[1] On the other hand, uric acid (UA), which has an antioxidant effect on the central nervous system (CNS), may play a protective role in onset and development of PD.[2,3] Gout, a consequence of hyperuricemia, is also associated with a lower risk of PD.[4] Previously, common dysfunctional variants of ATP-binding cassette transporter, sub-family G, member 2 (*ABCG2*, also known as *BCRP*), a urate transporter gene,[5,6] have been revealed to be a major cause of early-onset gout.[7] The common variant (Q141K, rs2231142) of *ABCG2* is proven to be a dysfunctional variant by in vitro functional studies.[5,6]

This study aimed to evaluate whether the Q141K variant of *ABCG2* could delay the age at onset (AAO) of PD in a relatively large population of Japanese patients.

Patients and Methods

Study participants

This study was approved by the institutional ethical committees, and all procedures involved in this study were performed in accordance with the Declaration of Helsinki. Informed consent in writing was obtained from each subject participating in this study. A total of 1015 PD patients (464 male and 548 female) and 507 gout male patients was collected and then genetically analyzed. PD patients were collected in Juntendo University (Tokyo, Japan) and Kobe University (Kobe, Japan). Diagnosis of PD was made by board-certified neurologists of the Japanese Society of Neurology, based on the presence of at least two cardinal features of PD with no secondary cause, no levodopa unresponsiveness, or no early signs of more extensive nervous system involvement.[8] Clinically defined gout cases were collected in the Kyoto Industrial Health Association (Kyoto, Japan).

Genetic analysis

Genomic DNA was extracted from whole peripheral blood cells.[9] For PD patients, genotyping of Q141K (rs2231142) in *ABCG2* gene was performed by direct sequencing using the following primers: forward, 5′-ATGGAGTTAACTGTCATTTGC-3′, and reverse, 5′-CACGTTCATATTATGTAACAAGCC-3′. DNA sequencing analysis was performed with a 3130xl Genetic Analyzer[10] (Life Technologies Corporation, Carlsbad, CA). The genotyping data of PD patients collected in Kobe University were obtained from the result of previous GWAS[11] using the Illumina Infinium HumanHap550 array (Illumina, Inc., San Diego, CA). For gout patients, genotyping of Q141K in *ABCG2* gene was performed by TaqMan assay (Life Technologies Corporation) with a LightCycler 480 (Roche Diagnostics, Mannheim, Germany).[12,13]

Statistical analysis

In the statistical analysis, SPSS v.17.0J (IBM Japan Inc., Tokyo, Japan) was used for all calculations. Regression analysis was used for the association analysis.

Results

The results of genotyping of gout and PD patients are shown in Table 1. Figure 1 shows the AAO of gout and PD participants of each genotype of *ABCG2* Q141K. The AAO (mean ± standard error) of gout were 40.4 ± 1.1 years old, 42.0 ± 0.7 years old, and 45.0 ± 1.1 years old for patients with Q141K homozygous (A/A), heterozygous (C/A) mutation, and without Q141K mutation (C/C), respectively. On the other hand, the AAO of PD were 58.5 ± 1.1 years old, 58.2 ± 0.5 years old, and 56.6 ± 0.5 years for patients with Q141K homozygous, heterozygous mutation, and without mutation, respectively. The AAO of gout with homozygous mutation was 4.6 years younger than those without Q141K mutation, while the AAO of PD with homozygous mutation was 1.6 years older than those without Q141K mutation.

The Q141K mutation of *ABCG2* hastened the onset of gout significantly ($P = 0.0027$; see Fig. 1A); on the contrary, this variant significantly delayed the PD onset ($P = 0.025$; see Fig. 1B).

Discussion

This study revealed for the first time that a common dysfunctional variant of *ABCG2* (Q141K, rs2231142) has surprisingly differential effects on two common diseases, significantly delaying the AAO of PD, while hastening that of gout. *ABCG2* encodes ATP-dependent transporter for urate excretion both in gut[14,15] and kidney.[16] Molecular functional studies revealed that ABCG2 dysfunction elevates serum UA levels.[5,6] As UA is the strong antioxidant, ABCG2 dysfunction might have a neuroprotective effect. In fact, our study showed that the dysfunctional variant of this UA-related gene, *ABCG2*, could have a protective effect against PD, which is wholly consistent with the previous studies suggesting that the higher levels of serum UA are negatively correlated with the risk of PD[17] and its rate of progression.[18]

So far, only a few genetic analyses have been performed about the association between PD onset and UA-related genes.[19,20] However, there is no report demonstrating that

Table 1. Genotype of *ABCG2* variant Q141K (rs2231142) for gout and PD patients.

	N (%)				
Q141K (rs2231142[1])	C/C	C/A	A/A	Total	MAF
Gout cases	131 (25.8)	257 (50.7)	119 (23.5)	507 (100.0)	0.49
PD cases	509 (50.1)	425 (41.9)	81 (8.0)	1015 (100.0)	0.29

PD, Parkinson's disease; MAF, minor allele frequency.
[1]For alleles of rs2231142 (C for cytosine; A for adenine), allele A is the minor allele.

a single variant of *ABCG2* could significantly affect the AAO of PD.

Together with the antioxidant effect of UA, our results strongly support the hypothesis that UA should reduce the risk of PD as an antioxidant, because oxidative stress is involved in the pathogenesis of PD. In addition to its expression in gut and kidney, ABCG2 highly expresses in the blood brain barrier (BBB).[21] Therefore, we propose a physiological model that ABCG2 exports urate from the brain side to the blood side at BBB (see Fig. 2). Since ABCG2 dysfunction decreases urate excretion via gut[14,15] and kidney,[16] which results in serum UA elevation,[5,6,14,16] it therefore has a pathogenic effect on earlier onset of gout. Elevated serum UA also should result in elevated UA levels in CNS. In addition, ABCG2 dysfunction could decrease urate excretion via BBB that enhances the

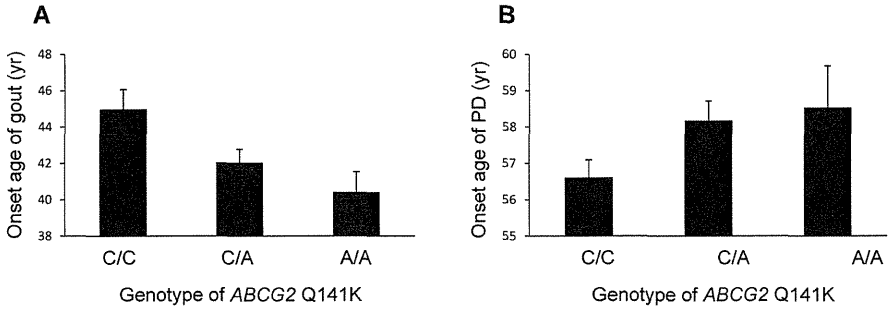

Figure 1. *ABCG2* dysfunctional variant (Q141K) and the age at onset (AAO) of gout/PD. The AAO of gout was significantly hastened as the number of minor alleles of Q141K increased ($P = 0.0027$); on the contrary, the AAO of PD was significantly delayed as the number of minor alleles of Q141K increased ($P = 0.025$). The AAO of gout with homozygous mutation (A/A) was 4.6 years younger than those without Q141K mutation (C/C). And the AAO of PD with homozygous mutation was 1.6 years older than those without Q141K mutation. Each bar represents the mean with standard error.

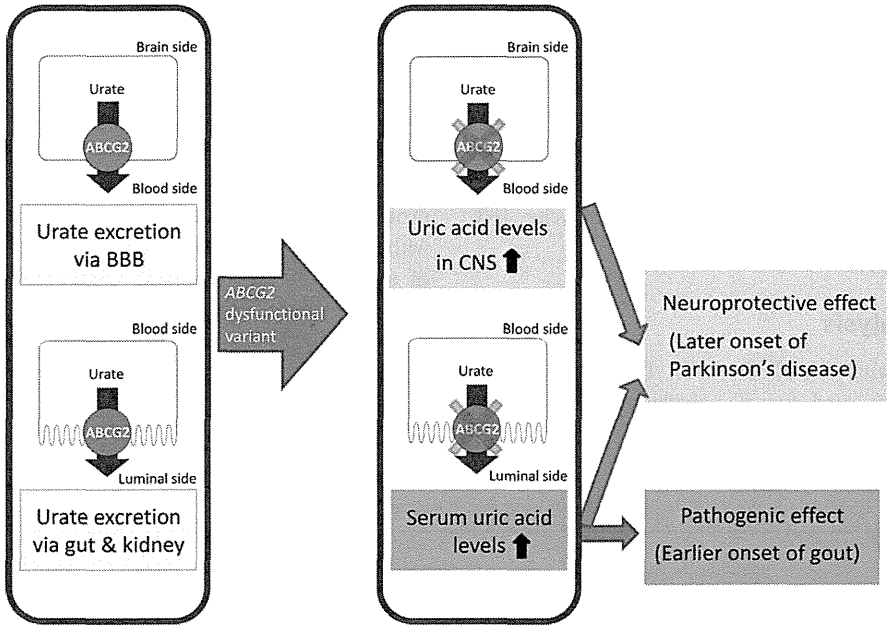

Figure 2. Contrary effects of ABCG2 dysfunction on PD and gout. ABCG2 is expressed in gut, kidney, and blood brain barrier (BBB) and exports urate. ABCG2 dysfunction in gut and kidney elevates the serum uric acid (UA) levels and subsequently causes gout. In this proposed model, ABCG2 dysfunction in BBB plays an important role on increasing UA levels in central nervous system (CNS), together with increased serum UA by ABCG2 dysfunction in gut and kidney.

elevation of UA levels in CNS as shown in our proposed model (see Fig. 2). In this model, ABCG2 dysfunction coordinately increases UA levels in CNS by the combined two differential mechanisms shown in Figure 2, although other UA-related gene variants have not been reported to have such differential mechanisms to elevate UA levels in CNS. Thus, the dysfunction of ABCG2 both in gut/kidney and BBB could cooperatively contribute to the elevated UA levels in CNS. These proposed differential mechanisms are consistent with our present result, which showed the differential effects on AAO of two common diseases, gout and PD. By these two differential mechanisms, therefore, ABCG2 dysfunction could have a significant neuroprotective effect for later onset of PD through increased UA, the strong antioxidant (see Fig. 2). That is why ABCG2 dysfunction could have significant effects on PD and be important in PD pathogenesis. Furthermore, the regulation of UA levels in serum and CNS could be applicable for prevention and therapy of PD.[22]

Acknowledgments

Supported by grants from the Ministry of Education, Culture, Sports, Science, and Technology of Japan, the Ministry of Health, Labour and Welfare of Japan, the Ministry of Defense of Japan, the Japan Society for the Promotion of Science, the Kawano Masanori Memorial Foundation for Promotion of Pediatrics, and the Gout Research Foundation of Japan. The authors thank all the participants involved in this study. We are also indebted to Y. Takada, T. Nakamura, H. Nakashima, Y. Sakurai, J. Abe, K. Gotanda, Y. Morimoto, H. Inoue, H. Ogata, S. Tatsukawa, Y. Shichijo, Y. Tanahashi, and A. Akashi, National Defense Medical College, Tokorozawa, Japan, for genetic analysis and enlightening discussion, and to T. Takada, the University of Tokyo Hospital, Tokyo, Japan, and Kimiyoshi Ichida, Tokyo University of Pharmacy and Life Sciences, Tokyo, Japan, for their helpful discussion.

Author Contribution

H. M., W. S., T. C., Y. K., A. N., S. S., M. S., T. T., and N. S. performed genetic analyses. H. T., W. S., H. O., M. F., K. N., T. S., K. Kaida., K. Kamakura., T. T., and N. H. performed clinical evaluations and medical record reviews. H. M. and T. C. wrote the paper. All authors contributed to data interpretation and manuscript preparation.

Conflicts of Interest

None declared.

References

1. Burkhardt CR, Weber HK. Parkinson's disease: a chronic, low-grade antioxidant deficiency? Med Hypotheses 1994;43:111–114.
2. Ascherio A, LeWitt PA, Xu K, et al. Urate as a predictor of the rate of clinical decline in Parkinson disease. Arch Neurol 2009;66:1460–1468.
3. Schlesinger I, Schlesinger N. Uric acid in Parkinson's disease. Mov Disord 2008;23:1653–1657.
4. Alonso A, Rodriguez LA, Logroscino G, Hernan MA. Gout and risk of Parkinson disease: a prospective study. Neurology 2007;69:1696–1700.
5. Woodward OM, Köttgen A, Coresh J, et al. Identification of a urate transporter, ABCG2, with a common functional polymorphism causing gout. Proc Natl Acad Sci USA 2009;106:10338–10342.
6. Matsuo H, Takada T, Ichida K, et al. Common defects of ABCG2, a high-capacity urate exporter, cause gout: a function-based genetic analysis in a Japanese population. Sci Transl Med 2009;1:5ra11.
7. Matsuo H, Ichida K, Takada T, et al. Common dysfunctional variants in ABCG2 are a major cause of early-onset gout. Sci Rep 2013;3:2014.
8. Bower JH, Maraganore DM, McDonnell SK, Rocca WA. Incidence and distribution of parkinsonism in Olmsted County, Minnesota, 1976–1990. Neurology 1999;52:1214–1220.
9. Matsuo H, Kamakura K, Saito M, et al. Familial paroxysmal dystonic choreoathetosis: clinical findings in a large Japanese family and genetic linkage to 2q. Arch Neurol 1999;56:721–726.
10. Chiba T, Matsuo H, Nagamori S, et al. Identification of a hypouricemia patient with SLC2A9 R380W, a pathogenic mutation for renal hypouricemia type 2. Nucleosides Nucleotides Nucleic Acids 2014;33:261–265.
11. Satake W, Nakabayashi Y, Mizuta I, et al. Genome-wide association study identifies common variants at four loci as genetic risk factors for Parkinson's disease. Nat Genet 2009;41:1303–1307.
12. Sakiyama M, Matsuo H, Shimizu S, et al. A common variant of leucine-rich repeat-containing 16A (LRRC16A) gene is associated with gout susceptibility. Hum Cell 2014;27:1–4.
13. Daimon M, Ji G, Saitoh T, et al. Large-scale search of SNPs for type 2 DM susceptibility genes in a Japanese population. Biochem Biophys Res Commun 2003;302:751–758.
14. Ichida K, Matsuo H, Takada T, et al. Decreased extra-renal urate excretion is a common cause of hyperuricemia. Nat Commun 2012;3:764.
15. Hosomi A, Nakanishi T, Fujita T, Tamai I. Extra-renal elimination of uric acid via intestinal efflux transporter BCRP/ABCG2. PLoS One 2012;7:e30456.

